

1 **Paradoxical neuronal hyperexcitability in a mouse model of mitochondrial pyruvate**  
2 **import deficiency**  
3

4 **Andres De la Rossa**<sup>1+</sup>, **Marine H. Laporte**<sup>1+</sup>, **Simone Astori**<sup>2+</sup>, Thomas Marissal<sup>3,4</sup>, Sylvie  
5 Montessuit<sup>1</sup>, Preethi Sheshadri<sup>5</sup>, Eva Ramos-Fernández<sup>2</sup>, Pablo Mendez<sup>6</sup>, Abbas Khani<sup>3</sup>,  
6 Charles Quairiaux<sup>3</sup>, Eric Taylor<sup>7</sup>, Jared Rutter<sup>8</sup>, José Manuel Nunes<sup>9</sup>, Alan Carleton<sup>3</sup>, Michael  
7 R. Duchen<sup>5</sup>, Carmen Sandi<sup>2\*</sup>, and Jean-Claude Martinou<sup>1\*</sup>.

8  
9 <sup>1</sup>Department of Cell Biology, University of Geneva. 1211 Geneva, Switzerland.

10 <sup>2</sup>Laboratory of Behavioral Genetics, Ecole Polytechnique Fédérale de Lausanne, Switzerland

11 <sup>3</sup>Department of Basic Neuroscience, University of Geneva. 1211 Geneva, Switzerland

12 <sup>4</sup>Institut de Neurobiologie de la Méditerranée, INSERM UMR1249, Université d'Aix-  
13 Marseille

14 <sup>5</sup>Department of Cell and Developmental Biology, University College London, London,  
15 WC1E 6BT

16 <sup>6</sup>Cajal Institute, Madrid, Spain.

17 <sup>7</sup>Department of Biochemistry and Fraternal Order of Eagles Diabetes Research Center, Carver  
18 College of Medicine, University of Iowa, Iowa City, IA USA

19 <sup>8</sup>Howard Hughes Medical Institute and Department of Biochemistry, University of Utah  
20 School of Medicine, Salt Lake City, UT, USA

21 <sup>9</sup>Department of Genetic and Evolution, University of Geneva, 1211 Geneva 4, Switzerland.

22

23 +Equal contribution; \*Corresponding Author: [jean-claude.martinou@unige.ch](mailto:jean-claude.martinou@unige.ch),  
24 [carmen.sandi@epfl.ch](mailto:carmen.sandi@epfl.ch)

25

26 **One Sentence Summary: Decreased OXPHOS and Ca<sup>2+</sup>-mediated neuronal**  
27 **hyperexcitability lead to seizure in a mouse model of mitochondrial pyruvate import**  
28 **deficiency.**

29

30 **Key words**

31 Mitochondrial pyruvate carrier (MPC), neuronal excitability, KCNQ (Kv.7) channels, M  
32 current, Glycolysis, Ketogenic diet (KD), β-hydroxybutyrate (βHB), CamKIIα-creERT2  
33 mice, Patch-clamp electrophysiology, epilepsy.

34

35 **Abstract**

36 A large number of neuropathologies, including cerebral ischemia and diverse  
37 mitochondriopathies, in which neurons experience a deficit in oxidative phosphorylation, and  
38 consequently in ATP, are frequently accompanied by severe seizures. This observation is  
39 paradoxical given that neuronal excitation imposes a high demand of ATP in neurons. The  
40 mechanisms underlying neuronal hyperexcitation in these pathologies remains unclear. Most  
41 of the ATP synthesized in neurons derives primarily from pyruvate-mediated oxidative  
42 phosphorylation, a process that relies on import of pyruvate into mitochondria occurring  
43 exclusively via the mitochondrial pyruvate carrier. To address the question of how  
44 neurons can be hyperexcitable with reduced levels of ATP, we generated mice in which the  
45 mitochondrial pyruvate carrier was genetically inactivated in adult glutamatergic neurons. We  
46 found that, despite decreased levels of oxidative phosphorylation in these excitatory neurons,  
47 mice were normal at rest. In response to mild inhibition of GABA mediated synaptic activity  
48 they rapidly developed severe seizures and died, whereas under similar conditions the  
49 behaviour of control mice remained unchanged. We show that neurons with a deficient  
50 mitochondrial pyruvate carrier are intrinsically hyperexcitable as a consequence of impaired  
51 calcium homeostasis, which reduces M-type potassium channel activity. Provision of ketone  
52 bodies restores energy status, calcium homeostasis and M-channel activity and attenuates  
53 seizures in animals fed a ketogenic diet.

54

55

## 56 **Introduction**

57 The brain is by far the main consumer of glucose and oxygen in the body, with pre- and post-  
58 synaptic mechanisms being the primary sites of ATP consumption(1-3). Most of the ATP in  
59 neurons is produced in mitochondria through pyruvate-mediated oxidative phosphorylation  
60 (OXPHOS), even though aerobic glycolysis, or the so-called Warburg effect, can generate  
61 sufficient ATP to sustain several neuronal functions, including neuronal firing(3-7). In  
62 neurons, pyruvate is produced either by glycolysis or through the action of lactate  
63 dehydrogenase, which mainly uses lactate derived from astrocytes(8). Whatever the source,  
64 pyruvate transport into mitochondria provides fuel for the tricarboxylic acid (TCA) cycle and  
65 boosts ATP production by OXPHOS.

66 Entry of pyruvate into mitochondria is totally dependent on the mitochondrial pyruvate carrier  
67 (MPC), a heterodimer composed of two subunits, MPC1 and MPC2 inserted into the inner  
68 mitochondrial membrane(9, 10). Deletion of MPC1 or MPC2 is sufficient to inactivate the  
69 carrier activity, and in the mouse causes embryonic lethality at E12(11, 12). Interestingly,  
70 providing ketone bodies, which directly feed the TCA cycle with acetyl-CoA and boost  
71 OXPHOS, to the pregnant females allowed the embryos to survive until birth(12). Besides  
72 energy production, glucose oxidation via the TCA cycle is also required for the synthesis of  
73 essential molecules, including the neurotransmitters glutamate and  $\gamma$ -aminobutyric acid  
74 (GABA). Therefore ATP production and neurotransmitter release are tightly linked to glucose  
75 and pyruvate metabolism. Accordingly, genetic pathologies linked to impaired glucose or  
76 pyruvate oxidation, such as mutations in the glucose transporter 1 (GLUT1)(13), pyruvate  
77 dehydrogenase (PDH)(13), MPC(14, 15), or complexes of the respiratory chain(16), result in  
78 severe synaptic dysfunction(17). Not surprisingly, these diseases are frequently associated  
79 with brain hypoactivity, although paradoxically they are often accompanied by neuronal  
80 hyperexcitability and behavioural seizures of varying severity. This raises the question of how

81 these paroxysmal, ATP consuming events can occur in patients despite a global brain energy  
82 deficit.

83 A likely explanation for the hyperexcitable phenotype is that seizures are due to an imbalance  
84 between inhibitory (mainly GABAergic) and excitatory (mainly glutamatergic) neuronal  
85 activity. While it is understandable that GABAergic neurons may release less inhibitory  
86 GABA in the pathologies mentioned above, it remains unclear how excitatory neurons with  
87 limited ATP production capacity can display hyperactivity leading to paroxysmic seizures  
88 within the context of low GABAergic neuronal activity.

89 To address this question, we inactivated the MPC in adult mice, specifically in CamKII $\alpha$ -  
90 expressing neurons (i.e. excitatory neurons) to reduce their OXPHOS capacity as previously  
91 shown(18, 19), and we analysed their electrical activity at rest and upon pharmacological  
92 inhibition of GABAergic transmission. This was achieved through genetic ablation of the  
93 MPC1 gene in adult mice using a tamoxifen-inducible system. Furthermore, by using  
94 CamKII $\alpha$ -Cre mice we were able to target the MPC1 deletion and study the impact of  
95 decreased pyruvate oxidation specifically in glutamatergic neurons. We found that, under  
96 resting conditions, mice lacking MPC1 in these excitatory neurons were indistinguishable  
97 from control mice in their general exploratory, social and stress-coping behaviors. In response  
98 to inhibition of GABA mediated synaptic activity they developed far more severe seizures  
99 than controls. We found that this phenotype was due to an intrinsic membrane  
100 hyperexcitability of MPC1-deficient glutamatergic neurons, which resulted from a calcium-  
101 mediated decrease in M-type K<sup>+</sup> channel activity. Strikingly, the hyperexcitability phenotype  
102 was reversed when the animals were maintained on a ketogenic diet.

103

104 **Results**

105 **MPC-deficient cortical neurons display decreased pyruvate-mediated oxidative**  
106 **phosphorylation in vitro.**

107 To assess the role of the mitochondrial pyruvate carrier (MPC) in neuronal OXPHOS, we first  
108 used primary cultures of cortical neurons largely depleted of astrocytes (Supplementary figure  
109 1a) and either RNA interference or pharmacological reagents to downregulate their MPC  
110 activity. To this end, two different shRNAs targeting MPC1 and three different  
111 pharmacological inhibitors of the carrier were used. Expression of either of the two shRNAs  
112 produced a significant reduction in MPC1 and MPC2 protein levels (the latter being unstable  
113 in the absence of MPC1) (Supplementary figure 1b, c). Both genetic and pharmacological  
114 impairment of MPC activity resulted in decreased pyruvate-driven basal and maximal oxygen  
115 consumption rates (OCR) (Figure 1a, Supplementary figure 1d) and decreased mitochondrial  
116 ATP production (Figure 1b), which is consistent with previously published results(18).  
117 Furthermore, mitochondrial membrane potential, measured using mitotracker and TMRE was  
118 significantly reduced in MPC-deficient neurons (Figure 1c, f). This was associated with an  
119 increased extracellular acidification rate (Supplementary figure 1e) and increased glucose  
120 uptake, which was measured using the 2-NBDG import assay (Supplementary figure 1f), two  
121 hallmarks of aerobic glycolysis.

122 We have previously reported that ketone bodies can restore normal OXPHOS in MPC-  
123 deficient murine embryonic fibroblasts(12). Consistent with this, we found that addition of the  
124 ketone body  $\beta$ -hydroxybutyrate ( $\beta$ HB) to the culture medium rescued all observed defective  
125 functionalities in MPC-deficient neurons, including oxygen consumption, ATP production,  
126 membrane potential (Figure 1d-f) and both extracellular acidification rate and glucose uptake  
127 (Supplementary figure 1g, h). Thus, we concluded that MPC-deficient neurons display low  
128 pyruvate-mediated oxidative phosphorylation and high aerobic glycolysis, both overcome

129 with  $\beta$ HB.

130

### 131 **Generation of mice with inducible MPC1 gene deletion in adult glutamatergic neurons**

132 Based on the results described above, and because neural excitation requires massive levels of  
133 ATP, we hypothesized that loss of MPC activity would reduce excitability especially in  
134 glutamatergic neurons that are high energy consumers(20). To test this hypothesis, we  
135 generated a mouse strain with an inducible deletion of the MPC1 gene, specifically in the  
136  $Ca^{2+}$ -calmodulin kinase II $\alpha$  (CamKII $\alpha$ )-expressing neurons, found predominantly in the  
137 hippocampus and cortex(21). We crossed MPC1<sup>flox+/flox+</sup> mice with the commercially  
138 available CamKII $\alpha$ -CreERT2 mice (Figure 2a). Induction of Cre activity by injection of  
139 Tamoxifen for 5 consecutive days resulted in deletion of MPC1 FLOXed alleles in the  
140 CamKII $\alpha$ -expressing adult neurons (Figure 2a). Hereafter, we refer to these mice as neuro-  
141 MPC1-KO. *In situ* immunofluorescence analyses showed a decrease in neuronal MPC1  
142 immunostaining in various layers of the cortex of neuro-MPC1-KO mice (Figure 2b).  
143 Western blot analysis of whole cortex, synaptosomes and mitochondria showed a significant  
144 decrease of both MPC1 and MPC2 in neuro-MPC1-KO mice compared to neuro-MPC1-WT  
145 mice (Figure 2c). Consistent with the results obtained with cultured neurons, we found that  
146 synaptosomes prepared from the cortex of neuro-MPC1-KO mice displayed lower oxygen  
147 consumption and imported higher amounts of glucose compared to synaptosomes from neuro-  
148 MPC1-WT mice (Supplementary figure 2a, b). Importantly, the lack of MPC1 did not affect  
149 the neuronal cell survival quantified either by counting the total number of cells, or by the  
150 number of apoptotic (TUNEL positive) cells (Supplementary figure 2c, d). At adulthood,  
151 both genotypes displayed similar body weight and lean mass composition (Supplementary  
152 figure 2e, f). At the behavioral level, adult neuro-MPC1-KO mice showed a tendency toward

153 lower anxiety-like behaviors, but no difference in general locomotion, sociability or stress-  
154 coping behaviors (Supplementary figure 2g-j).

155 These data indicate that, under resting conditions, the excitatory neurons in most adult mice  
156 have the ability to bypass the MPC to meet their metabolic demands.

157

158 **Neuro-MPC1-KO mice are highly sensitive to pro-convulsant drugs and develop acute**  
159 **epileptic-like seizures**

160 The output activity of a neuron results from the balance between the excitatory and the  
161 inhibitory inputs it receives. Perturbation of this delicate balance can lead to severe seizures  
162 as a result of exacerbated, uncontrolled neuronal firing. To test whether OXPHOS-deficient  
163 excitatory neurons could sustain intense neuronal firing, we challenged neuro-MPC1-KO  
164 adult mice, with either pentylentetrazole (PTZ), a GABA receptor antagonist, or kainic acid,  
165 an activator of glutamate receptors. We used the PTZ kindling protocol described  
166 previously(22), in which a sub-convulsant dose (35mg/kg) of PTZ is injected intraperitoneally  
167 (ip) once every two days on a period of 15 days (Figure 3a). Phenotypic scoring after each  
168 PTZ injection in neuro-MPC1-WT mice showed a progressive sensitization (kindling) starting  
169 with hypoactivity after the first injection (scored as 1); a few brief and transient muscle  
170 contractions (jerks, scored as 2) or appearance of tail rigidity (Straub's tail, scored as 3)  
171 following the second or third injection; and convulsive status epilepticus (scored as 6) after  
172 the 6<sup>th</sup> or 7<sup>th</sup> injection (Figure 3a, b). In contrast, all neuro-MPC1-KO mice developed severe,  
173 prolonged seizures (score 6) within 10 min of the first PTZ injection (Figure 3b) and all died  
174 during seizures within the next three PTZ injections (Supplementary figure 3a). When mice  
175 were injected with 20 mg/kg kainic acid, a similar hypersensitivity (score 6) was observed in  
176 neuro-MPC1-KO mice indicating that this sensitivity is not restricted to PTZ (Supplementary  
177 figure 3b).

178 In a parallel series of experiments, and in order to assess the specificity of our results to  
179 excitatory neurons, we investigated the effects of PTZ in mice in which MPC1 was deleted in  
180 adult astrocytes (hereafter termed astro-MPC1-KO mice) (Supplementary figure 3c-e). In  
181 contrast to neuro-MPC1-KO mice, astro-MPC1-KO mice showed the same response as  
182 control animals following PTZ injection (Supplementary figure 3f, g), indicating that the  
183 phenotype observed in neuro-MPC1-KO mice is linked to the deletion of MPC1 in excitatory  
184 neurons.

185 To characterize the seizure symptoms in more detail, we recorded the electrical activity in the  
186 brains of neuro-MPC1-WT and neuro-MPC1-KO mice by electroencephalogram (EEG)  
187 following a single injection of PTZ (Figure 3c). In neuro-MPC1-KO mice, rhythmic EEG  
188 patterns emerged within 5-10 minutes after PTZ injection, invading all electrodes (Figure 3c).  
189 These electrical patterns coincided with the occurrence of behavioural manifestations of  
190 seizures, i.e. tonic-clonic movements. Rapidly thereafter, large spike and wave discharges  
191 developed, again invading all surface electrodes and coinciding with numerous fast ripples  
192 (Figure 3c, inset). Such EEG patterns are characteristic of seizure episodes in humans and  
193 were not observed in the PTZ-injected neuro-MPC1-WT mice. These data indicate that neuro-  
194 MPC1-KO mice develop an epilepsy-like phenotype following administration of a single sub-  
195 convulsant dose of PTZ.

196 We also tested whether we could reproduce the seizure phenotype using hippocampal  
197 organotypic cultures from  $\text{CamKII}\alpha\text{-CreERT2}^+\text{-MPC1}^{\text{Flox}/\text{Flox}}$  mice exposed to PTZ,  
198 combined with calcium imaging. Individual neurons in hippocampal slices from both WT and  
199 KO mice exhibited spontaneous calcium activity throughout the duration of the recordings  
200 (Figure 3d, e and videos 1 and 2) although, interestingly, the frequency of calcium events, as  
201 well as the number of co-activation events (i.e. neuronal synchronizations above chance  
202 levels) generated in MPC1-deficient neurons were significantly higher than those generated in



203 MPC1-WT neurons (Figure 3f, g and videos 1 and 2). In contrast, neither the amplitude nor  
204 the duration of the discharges was modified (Figure 3h, i). These results suggest that neuro-  
205 MPC1-KO neurons are more active and are more often recruited into synchronized patterns  
206 associated with the epileptic activity.

207

### 208 **Inhibition of PTZ-induced seizures in neuro-MPC1-KO mice by the ketogenic diet**

209 The ketogenic diet (KD) has been reported to decrease seizures in patients with  
210 pharmacologically refractory epilepsy(23). Ketone bodies, mainly generated by the liver  
211 during fasting and hypoglycaemia, are used by neurons to provide the TCA cycle with acetyl-  
212 CoA, normally provided by pyruvate dehydrogenase-mediated oxidation of pyruvate. Thus,  
213 ketone bodies ensure that oxidative phosphorylation and ATP production is maintained in  
214 neurons in conditions of glucose starvation. We tested whether a ketogenic diet could prevent  
215 PTZ-induced seizures in neuro-MPC1-KO mice. As previously reported(24), we found that  
216 the KD produces a decrease in glycaemia and an increase in the blood level of 3- $\beta$ -hydroxy-  
217 butyrate ( $\beta$ HB), one of the three major ketone bodies generated by the liver (Supplementary  
218 figure 4a, b). In addition, we found that mice fed on the KD for one week were completely  
219 resistant to PTZ injection (Figure 4a). Supplementing the drinking water with 1%  $\beta$ HB was  
220 sufficient to prevent PTZ-induced seizures (Figure 4b). Similarly, ip administration of  $\beta$ HB  
221 15 minutes before PTZ injection, or starvation overnight, both of which conditions led to  
222 increased  $\beta$ HB blood levels (Supplementary figure 4c-e), significantly reduced the PTZ-  
223 induced clinical score of neuro-MPC1-KO mice (Figure 4b, c). These results indicate that the  
224 phenotype displayed by the neuro-MPC1-KO mice is mainly metabolic in origin and is  
225 unlikely to be the consequence of neuronal network remodelling.

226

227 **MPC1-deficient neurons display intrinsic hyperexcitability, which is prevented by**  
228 **ketone bodies**

229 To investigate the cellular mechanisms that might mediate the sensitivity of neuro-MPC1-KO  
230 mice to pro-convulsant drugs, we examined the electrophysiological properties of MPC1-  
231 deficient neurons. To this end, we performed whole-cell patch clamp recordings in acute  
232 hippocampal slices from neuro-MPC1-KO mice and their neuro-MPC1-WT littermates. CA1  
233 pyramidal cells from neuro-MPC1-KO mice exhibited higher discharge frequency compared  
234 to neurons from neuro-MPC1-WT mice when firing was elicited by somatic injections of  
235 current ramps of increasing amplitude (Figure 5a, b). Neurons from neuro-MPC1-KO mice  
236 required less current injection (rheobase, Figure 5c) to reach the firing threshold, which was  
237 more hyperpolarized when compared to neuro-MPC1-WT cells (Figure 5d). Similarly,  
238 MPC1-KO neurons displayed higher firing when depolarization was induced with squared  
239 current pulses (Supplementary figure 5a, b).

240 Next, we asked whether ketone bodies, which as shown in Figure 4 prevent PTZ-induced  
241 seizures, could modulate neuronal excitability and restore normal cell discharges in neuro-  
242 MPC1-KO mice. For these experiments, we first recorded action potential firing under control  
243 conditions, and then perfused the slices with  $\beta$ HB (2 mM, >20 min exposure). As shown in  
244 Figure 5, whereas cell firing was unaltered in neuro-MPC1-WT cells (Figure 5e, f),  $\beta$ HB  
245 reduced excitability in pyramidal cells from the neuro-MPC1-KO mice (Figure 5g, h). Control  
246 experiments showed that cell excitability from both genotypes was unchanged during  
247 prolonged recordings (Figure 5f, h), confirming that the change in neuro-MPC1-KO firing  
248 was not due to a rundown in cellular excitability caused by, e.g., cell dialysis.

249 Taken together, these results indicate that ketone bodies reduce the intrinsic hyperexcitability  
250 of glutamatergic cells from neuro-MPC1-KO mice, providing a plausible explanation for the  
251 protective effect of the KD against PTZ-induced seizures.

252

253 **MPC1-deficient neurons display altered M-type potassium channel activation, which is**  
254 **corrected by  $\beta$ -hydroxybutyrate**

255 To gain insight into the mechanisms governing neuronal hyperexcitability, we analysed the  
256 cellular passive properties and action potential characteristics of all recordings performed in  
257 cells from neuro-MPC1-KO and neuro-MPC1-WT mice (Supplementary figure 5c-k). The  
258 reduction in rheobase and the shift in threshold potential induced by MPC1 deletion were  
259 accompanied by several changes in passive and active membrane properties governing cell  
260 excitability, including a significant increase in the input resistance ( $R_i$ ) and in the voltage  
261 response to a depolarizing current injection ( $\text{depol}_{\text{sub}}$ ), along with a marginally significant  
262 reduction in HCN channel-mediated sag (Supplementary figure 5c-i). The fast  
263 afterhyperpolarization (fAHP) accompanying action potentials was not altered, ruling out a  
264 major contribution of BK channels (Supplementary figure 5j). However, the medium  
265 afterhyperpolarization (mAHP), measured as the negative peak of the voltage deflection at the  
266 offset of the depolarizing ramps was significantly reduced in cells from neuro-MPC1-KO  
267 mice (Supplementary figure 5k). In CA1 pyramidal cells, mAHP is primarily mediated by the  
268 activation KCNQ2/3 (Kv7.2 and Kv7.3) channels, which generate an M-type  $K^+$  conductance  
269 regulating intrinsic excitability and synaptic integration(25, 26). Opening of these channels  
270 produces an outward potassium current that functions as a ‘brake’ for neurons receiving  
271 persistent excitatory input(27). Consistently, mutations in KCNQ2/3 genes have been  
272 associated with seizures in the mouse(28), as well as in patients(29, 30), pointing to these  
273 channels as interesting targets for anticonvulsant therapy(31). To verify whether neuro-  
274 MPC1-KO mice display an altered contribution of the M-type  $K^+$  conductance, we tested the  
275 effect of the M-type channel blocker XE991 (10  $\mu\text{M}$ ) on CA1 pyramidal cell firing. XE991  
276 led to a significant increase in firing frequency of neuro-MPC1-WT cells, whereas firing of

277 neuro-MPC1-KO cells was not significantly modified (Figure 5i, j). Consistently, XE991  
278 induced a significant reduction in the rheobase and a shift in the threshold potential in neuro-  
279 MPC1-WT cells, but had no impact on neuro-MPC1-KO cells (Figure 5k, l), pointing to a  
280 limited activity of KCNQ2/3 channels in these neurons. Interestingly, bath application of  $\beta$ HB  
281 following KCNQ2/3 channel blockade with XE991 failed to reduce the hyperexcitability of  
282 neuro-MPC1-KO mice (Figure 5j-l). We also noticed that, in the absence of XE991, the  
283 reduction of intrinsic excitability by  $\beta$ HB in MPC-deficient neurons was accompanied by a  
284 significant increase in mAHP (Figure 5m, n), suggesting that  $\beta$ HB may potentiate the  
285 recruitment of the M-type  $K^+$  channels. Moreover, the M-type channel activator retigabine (10  
286  $\mu$ M) effectively decreased the hyperexcitability of pyramidal cells from neuro-MPC1-KO  
287 mice to a level that was no further affected by  $\beta$ HB (Figure 5o, p). This suggests that  $\beta$ HB  
288 and retigabine display a similar mechanism of action, which is consistent with recent findings  
289 showing that  $\beta$ HB can directly bind to and activate KCNQ2/3 channels(32).

290 We finally tested whether the increased neuronal excitability in neuro-MPC1-KO mice was  
291 also accompanied by alterations in glutamatergic transmission. In acute slices, we recorded  
292 field potentials in CA1 stratum radiatum elicited by electrical stimulation of the Schaffer  
293 collaterals (Supplementary figure 5l). No overt genotype differences were found in the input-  
294 output curves of field excitatory postsynaptic potentials (fEPSPs), and the lack of changes in  
295 paired-pulse ratio indicated no major alteration in the presynaptic release (Supplementary  
296 figure 5m, n).

297 Altogether, these results indicate that the hyperexcitability of CA1 pyramidal neurons from  
298 neuro-MPC1-KO mice is mediated by alterations in intrinsic cell excitability associated with a  
299 reduced M-type  $K^+$  channel activation, with no major changes in excitatory synaptic inputs.

300

301

## 302 **Alteration of calcium homeostasis in MPC1-deficient neurons**

303 The conductance of KCNQ channels is regulated by phosphatidylinositol-4,5-bisphosphate  
304 (PIP<sub>2</sub>) and calmodulin (CaM)(33, 34). In particular, reduction in free CaM in hippocampal  
305 neurons decreases M-current density and increases neuronal excitability(35, 36). Thus,  
306 calcium can trigger loss of interaction of CaM and KCNQ2/3 channels, leading to M-type  
307 current suppression(37).

308 We tested whether disruption of calcium homeostasis could be responsible for the deficit in  
309 the M-type K<sup>+</sup> channel activity displayed by MPC1-deficient neurons. We first assess whether  
310 calcium homeostasis was perturbed in MPC-deficient cortical neurons in vitro. Using the  
311 fluorimetric calcium probes Fura2-AM and the low affinity FuraFF-AM and live cell  
312 imaging, we found a significant increase in the peak concentration of cytosolic calcium upon  
313 depolarization of both control and MPC-deficient neurons in response to either glutamate (10  
314 μM) or KCl (50 mM) (Figure 6a-c; Supplementary figure 6a-d). However, while the peak of  
315 calcium concentration was transient in control neurons, and returned to basal levels, both the  
316 magnitude and duration of the calcium elevation were greater in MPC-deficient neurons  
317 (Figure 6a, Supplementary figure 6d, Wash). Interestingly, the long lasting increased calcium  
318 level in MPC-deficient neurons was abolished by addition of 10 mM βHB to the culture  
319 medium 30 min prior to recording (Figure 6a-c). Together these results show that loss of MPC  
320 activity leads to a significant increase of cytosolic calcium levels in depolarized neurons.

321 Mitochondria import calcium through the mitochondrial calcium uniporter (MCU) in a  
322 membrane potential dependent manner and thereby play a major role in calcium  
323 homeostasis(38). In an interesting study published during the preparation of this manuscript, it  
324 was reported that inhibition of the MPC in cardiomyocytes and hepatocytes can result in  
325 higher expression of the MCU gatekeeper MICU1 and inhibition of MCU-mediated calcium  
326 uptake(39). However, our investigations did not validate this hypothesis (Supplementary

327 figure 7). Therefore, we focused our study on the mitochondrial membrane potential, which  
328 we found reduced in the MPC-deficient neurons (Figure 1c, f), and which could affect the  
329 buffering capacity of mitochondria upon stimulation. This hypothesis was tested using Fura2-  
330 loaded cultured cortical neurons at rest or upon stimulation with KCl, in the presence or  
331 absence of chemical inhibitors of the MPC. These experiments confirmed that the peak and  
332 duration of calcium concentration in the cytosol were significantly increased in MPC-  
333 deficient neurons (Figure 6d-f). The mitochondrial uncoupler FCCP was then added to the  
334 cultures to release the calcium retained in the mitochondria. The amount of calcium released  
335 from MPC-deficient mitochondria by FCCP was significantly lower than in wild type controls  
336 (Figure 6d-f), suggesting that the capacity of mitochondria to import and store calcium was  
337 decreased in these neurons. Moreover, the elevation of cytosolic calcium seen in MPC-  
338 deficient neurons was recapitulated in WT neurons following the addition of RU360, an  
339 inhibitor of the MCU (Figure 6d-f). To further test whether the increased cytosolic calcium  
340 resulting from dysfunctional mitochondria was responsible for the hyperexcitability of MPC1-  
341 deficient neurons, we performed electrophysiological recordings in CA1 pyramidal cells in  
342 presence of RU360 into the patch pipette. In neuro-MPC1-WT cells, addition of 1  $\mu$ M or 10  
343  $\mu$ M RU360 to the cell pipette caused an increase in cell firing (Figure 6g, h) while 10  $\mu$ M  
344 RU360 had no effect in neuro-MPC1-KO cells (Figure 6i, j). Importantly, blockade of the  
345 MCU with RU360 in neuro-MPC1-WT cells was accompanied by a significant reduction in  
346 the mAHP (Figure 6k, l), indicating that calcium alterations induced by mitochondrial  
347 dysfunction may indeed affect M-type  $K^+$  channel activation. Finally, whereas  $\beta$ HB treatment  
348 did not significantly alter the firing of neuro-MPC1-WT cells in control conditions (Figure 5e,  
349 f), it reduced the excitability of cells infused with 10  $\mu$ M RU360 while slightly increasing  
350 mAHP (Figure 6 m, n), consistent with the hypothesis that  $\beta$ HB normalizes the alteration in  
351 the M-type  $K^+$  conductance.

352 Altogether, our results show that MPC1-deficient neurons display a lower mitochondrial  
353 calcium buffering capacity which may explain the hypoactivity of the M-type  $K^+$  channel and  
354 the intrinsic hyperexcitability of neurons.

355

356 **Discussion**

357 One of the main questions in the field of neuropathology is how patients with mutations or  
358 pathologies resulting in major OXPHOS deficit, including cerebral ischemia or diverse  
359 mitochondriopathies, develop severe seizures, i.e. clinical symptoms that result from intense,  
360 energy consuming, neuronal firing. A likely explanation is that seizures are due to an  
361 imbalance between inhibitory and excitatory neuronal activity, which could result from  
362 decreased inhibitory neuronal transmission. However, this explanation is not entirely  
363 satisfactory since it does not explain how, even in this context, energy-deficient excitatory  
364 neurons can display hyperactivity and sustain a high firing rate. Understanding the  
365 mechanism underlying this hyperexcitability is important and could lead to novel treatments  
366 for these convulsive and often life-threatening events.

367 To address this question, we inactivated the MPC specifically in adult CamKII $\alpha$ -expressing  
368 neurons in the mouse to decrease OXPHOS, as previously reported(18)(40), and in the same  
369 mice we inhibited the GABAergic transmission pharmacologically. We found that, despite  
370 decreased OXPHOS in glutamatergic neurons, these mice appeared normal at rest and  
371 presented a normal behavioral repertoire (i.e., novelty exploration, sociability, stress coping),  
372 except for lower anxiety-like behaviors which are consistent with a higher glutamatergic  
373 tone(41). However, they developed severe seizures immediately following low level  
374 administration of two pro-convulsant drugs, the GABA receptor antagonist pentylentetrazole  
375 (PTZ), or the glutamate receptor agonist kainic acid.

376 The lack of an apparent phenotype in neuro-MPC1-KO mice under resting conditions  
377 suggests that, up to a certain point, mitochondria can compensate for the deficit in  
378 mitochondrial pyruvate import by using other substrates to fuel the TCA cycle. Recently,  
379 Timper et al. (2018)(42) reported that proopiomelanocortin (POMC)-expressing neurons, in  
380 which OXPHOS was impaired either by partial inactivation of Apoptosis-Induced Factor or



381 by deletion of MPC1, were able to rewire their metabolism towards mitochondrial fatty acid  
382 oxidation to stimulate mitochondrial respiration. However, it seems unlikely that such a  
383 compensatory mechanism can occur in MPC1-deficient glutamatergic neurons since these  
384 neurons do not express the enzymes necessary for  $\beta$ -oxidation of fatty acids(43). Furthermore,  
385 it is unlikely that the astrocyte-neuron-shuttle, which supplies astrocyte-derived lactate to  
386 neurons to boost OXPHOS(44), can circumvent the loss of the MPC since all available data  
387 thus far indicate that lactate must first be converted by neuronal LDH into pyruvate in order to  
388 fuel the TCA cycle.

389 Instead, our data point toward aerobic glycolysis as a likely compensatory mechanism for the  
390 OXPHOS deficit as several studies have reported that increased glycolysis at the synapse,  
391 uncoupled from oxidative phosphorylation, could provide sufficient ATP to ensure normal  
392 neurotransmission(6, 45). It is therefore possible that, under resting conditions, increased  
393 aerobic glycolysis participates in the activity of MPC1-deficient glutamatergic neurons.

394 Despite the lack of an obvious phenotype in resting mice, we found that, when challenged  
395 with the pro-convulsant molecules PTZ or kainic acid, the neuro-MPC1-KO mice were far  
396 more sensitive than WT animals and rapidly exhibited severe acute seizures. This suggests  
397 that the basal electrical activity of MPC1-deficient neurons may be continuously  
398 counterbalanced by inhibitory synapses, providing the normal resting phenotype described  
399 above. However, upon release of the 'brakes' exerted by the inhibitory system, the neuro-  
400 MPC1-KO neurons would become hyperactive, which would translate into the observed  
401 epileptic output. Consistent with our data, mice deficient in pyruvate dehydrogenase (PDH),  
402 the enzyme acting immediately downstream of the MPC, were found to display an  
403 epileptiform cortical activity accompanied by behaviorally observable seizures(46). In this  
404 case, the epileptiform activity occurred in the context of reduced background cortical  
405 activation and, as suggested by the authors, the most likely explanation was that seizures

406 resulted from a combination of decreased activity of inhibitory neurons, mostly parvalbumin-  
407 expressing cortical neurons, with slightly overexcitable excitatory neurons. Similar to PDH-  
408 deficient neurons, we found that the MPC1-deficient neurons displayed higher input  
409 resistance and increased spike frequency after stimulation, a phenotype that we investigated  
410 further and found to be mediated by an impairment of the medium component of the after-  
411 hyperpolarization potential mediated by an M-type K<sup>+</sup> conductance.

412 K<sup>+</sup> efflux is the primary force behind the cellular repolarization that limits the spike after  
413 depolarization and thereby prevents neuronal hyperexcitability. One important class of K<sup>+</sup>  
414 channels that fulfills this task is the M-current (*I<sub>M</sub>*)-generating KCNQ channel family (also  
415 called Kv7 channels)(47). In hippocampal neurons the *I<sub>M</sub>* is mediated by the KCNQ2 and  
416 KCNQ3 channels (Kv7.1 and Kv7.2), which form hetero or homodimers. Loss of function of  
417 KCNQ2 or KCNQ3 causes epilepsy in humans and mice(28, 48-50). In support of the notion  
418 that these channels underlie the intrinsic membrane hyperexcitability of MPC1-KO neurons,  
419 we found that inhibition of these channels using the small molecule XE991 did not change the  
420 electrical properties of KO neurons, while it made WT neurons more excitable. Our results  
421 suggest that KCNQ2/3 channels are closed in MPC1-deficient neurons, and that this could  
422 underlie their hyperexcitability. The reason for the silencing of these channels appears to be  
423 linked to an excess of cytosolic calcium. The calcium binding protein, Calmodulin (CaM), has  
424 been shown to bind to the C-terminal part of the KCNQ channel and to be required for its  
425 activity(35). Intracellular calcium decreases CaM-mediated KCNQ channel activity(33, 37)  
426 by detaching CaM from the channel or by inducing changes in configuration of the  
427 calmodulin-KCNQ channel complex(37). Importantly, increasing cytosolic calcium levels in  
428 wild type neurons from acute hippocampal slices, using the MCU inhibitor RU360, was  
429 sufficient to increase their firing properties, while RU360 had no significant effect on the  
430 excitability of the neuro-MPC1-KO neurons. The increased intracellular levels of calcium in

431 neuro-MPC1-KO neurons probably result from a decreased capacity of mitochondria to buffer  
432 cytosolic calcium. Such a reduction in calcium buffering is likely to be the consequence of a  
433 reduced mitochondrial membrane potential, directly linked to a decreased oxygen  
434 consumption and OXPHOS. It is known that cells with low respiratory capacity consume  
435 ATP through the ATP synthase to maintain a minimal mitochondrial membrane potential that  
436 allows them to survive(51). Accordingly, ketone bodies, which restore oxygen consumption,  
437 ATP production, and mitochondrial membrane potential, reduce the excitability of neuro-  
438 MPC1-KO neurons. In addition our study suggest that  $\beta$ HB could act directly on the M-  
439 channel, as previously reported by Manville et al.,(32) .

440 In conclusion, using mice carrying an inducible deletion of the MPC specifically in excitatory  
441 neurons, our data revealed a complex link between mitochondrial metabolism, calcium  
442 homeostasis, M-channel activity and glutamatergic neuron excitability. Our study  
443 complements that of Jakkamsetti et al.(46) who reported the impact of PDH deficiency on  
444 brain activity focusing primarily on the inhibitory system and less on the excitatory system as  
445 we do here. We have shown that, despite impaired pyruvate-mediated OXPHOS,  
446 glutamatergic neurons can sustain high firing and can trigger severe behaviourally observable  
447 seizures when the GABAergic network is inhibited. Therefore, the paradoxical seizures that  
448 frequently occur in pathologies associated with decreased OXPHOS, whether they be the  
449 consequence of impaired glucose metabolism, or genetically mediated mitochondriopathies,  
450 could result from either hypoactivity of inhibitory neurons and/or hyperactivity of excitatory  
451 neurons. We find that calcium-mediated closure of KCNQ channels promotes membrane  
452 hyperexcitability on excitatory neurons, suggesting that therapeutic modulation of KCNQ  
453 channels may offer an interesting therapeutic approach to prevent seizures occurring in  
454 metabolic diseases with reduced OXPHOS.

## 455 **Material and Methods**

### 456 **Study design**

457 Data sources from mice included in vivo (behavioural tests, pro-convulsant drug injections,  
458 electroencephalogram), brain slice recordings of neuronal activity and electrophysiology,  
459 isolation of synaptosomes and primary culture of cortical neurons. For mouse experiments,  
460 pilot data from three or four samples per group provided an estimate of SD and effect  
461 magnitude, which, together with a power of 0.8 and  $P < 0.05$ , guided sample sizes using the  
462 G\*power software (G\*power version 3.1.9.6.). MPC1-WT and MPC1-KO mice from the  
463 same litter were randomly selected for experiments. Replicates and statistical tests are cited  
464 with each result. All procedures were approved by the Institutional Animal Care and Use  
465 Committee of the University of Geneva and with permission of the Geneva cantonal  
466 authorities. Data analysis was blind and performed concurrently on control and experimental  
467 data with the same parameters. No data, including outlier values, were excluded.

468

### 469 **Mice**

470 The CamKII $\alpha$ -CreERT2 mouse was obtained from Jackson (stock number 012362). The  
471 MPC1<sup>Flox/Flox</sup> mouse was a gift from professor Eric Taylor (University of Iowa)(Gray). The  
472 Ai14 reporter mouse was a gift from professor Ivan Rodriguez (University of  
473 Geneva)(Madisen). The GFAP-CreERT2 mouse was a gift from professor Nicolas Toni  
474 (University of Lausanne)(52). By using the Cre driver lines, we generated two different cell-  
475 type specific MPC1-KO mice: CamKII $\alpha$ -CreERT2<sup>+</sup>-MPC1<sup>Flox+/Flox+</sup> mice (here called neuro-  
476 MPC1-KO) in which MPC1 was knocked out specifically in excitatory glutamatergic  
477 neurons; and GFAP-CreERT2<sup>+</sup>-MPC1<sup>Flox+/Flox+</sup> mice in which MPC1 is knockout specifically  
478 in astrocytes (here called astro-MPC1-KO). In all experiments age-matched wild type controls  
479 were used and are referred to in the text as neuro-MPC1-WT (CamKII $\alpha$ -CreERT2<sup>-</sup>-

480 MPC1<sup>Flox+/Flox+</sup>) and astro-MPC1-WT mice (GFAP-CreERT2<sup>-</sup>-MPC1<sup>Flox+/Flox+</sup>). The neuro-  
481 MPC1-KO and astro-MPC1-KO phenotypes were tamoxifen-inducible. In order to induce  
482 MPC1 deletion, the mice were injected intraperitoneally (ip) for 5 consecutive days with  
483 100µl of 10mg/ml tamoxifen (Sigma, 85256) in sunflower oil. The mice were considered to  
484 be MPC1-KO from one week after the final injection. All experiments were carried out in  
485 accordance with the Institutional Animal Care and Use Committee of the University of  
486 Geneva and with permission of the Geneva cantonal authorities (Authorization numbers  
487 GE/42/17, GE/70/15, GE/123/16, GE/86/16, GE/77/18, GE/205/17) and of the Veterinary  
488 Office Committee for Animal Experimentation of Canton Vaud (Authorization number  
489 VD3081).

490

#### 491 **Pentylenetetrazol (PTZ)-induced convulsion protocol**

492 We used the PTZ kindling model of epilepsy as described in Dhir et al.,(22). Briefly, this test  
493 entails chronic intraperitoneal (ip) injection of 35 mg/kg PTZ (Sigma, P6500), which is a sub-  
494 convulsant dose for WT mice, every 2 days for 2 weeks, and after each PTZ injection, the  
495 mice were scored according to their clinical symptoms, as described in previously (22)(53).  
496 After each PTZ injection, the animals were gently placed in isolated transparent plexiglass  
497 cages and their behaviour was observed to assign a seizure score based on the following  
498 criteria: stage 1: sudden behavioral arrest and/or motionless staring; stage 2: jerks; stage 3:  
499 Straub's tail (rigid tail being held perpendicularly to the surface of the body); stage 4: partial  
500 clonus in a sitting position; stage 5: generalized clonus; stage 6: convulsions including clonic  
501 and/or tonic-clonic seizures while lying on the side and/or wild jumping (convulsive status  
502 epilepticus). Mice were scored over a period of 30 min and the tests were performed in semi-  
503 blind mode (carried out by 2 experimenters of which only one knew the genotype). After the  
504 PTZ test, mice were immediately sacrificed in a CO<sub>2</sub> chamber. The seizure severity score was

505 calculated by taking the sum of the behavior and seizure patterns for all animals in a group  
506 and dividing by the number of animals present in the group.

507

### 508 **Electroencephalogram (EEG)**

509 Surface EEGs were recorded in head-fixed, awake animals with 32 stainless steel electrodes  
510 (500  $\mu\text{m}$   $\varnothing$ ) covering the entire skull surface as described previously(54, 55). Briefly, a head-  
511 post was placed under isoflurane anaesthesia allowing head-fixation. Recording sessions took  
512 place after a period of 4 days of head-fixation training to allow acclimatization of the animals  
513 to the experimental setup. PTZ was injected ip at the beginning of the session.  
514 Electrophysiological differential recordings were acquired with a Digital Lynx SX  
515 (Neuralynx, USA) at a sampling rate of 4 kHz and with a 2kHz low-pass. The ground  
516 electrode was placed above the nasal bone and the reference electrode was placed on the  
517 midline between parietal bones (channel 31, Figure 3C). All signals were calculated against  
518 the average reference offline.

519

### 520 **Patch-clamp electrophysiology**

521 Tamoxifen-treated MPC1Flox/Flox-CamKII $\alpha$ Cre(+) mice and wild-type littermates (6-10  
522 weeks-old) were anaesthetized with isoflurane and decapitated, and the brain was quickly  
523 removed and placed in oxygenated (95% O<sub>2</sub> / 5% CO<sub>2</sub>) ice-cold N-Methyl-D-glucamine  
524 (NMDG)-based medium, containing (in mM): 110 NMDG, 2.5 KCl, 1.2 NaH<sub>2</sub>PO<sub>4</sub>, 30  
525 NaHCO<sub>3</sub>, 20 HEPES, 10 MgCl<sub>2</sub>, 0.5 CaCl<sub>2</sub>, 25 glucose, 5 L(+)-ascorbic acid, 2 thiourea, 3  
526 Na-pyruvate (titrated to pH 7.2-7.3 with HCl). Acute hippocampal transverse slices (350  $\mu\text{m}$   
527 thick) were cut using a vibrating tissue slicer (Campden Instruments). Slices recovered for 1 h  
528 at 35°C and subsequently at room temperature in a storage solution containing (in mM): 92  
529 NaCl, 2.5 KCl, 1.2 NaH<sub>2</sub>PO<sub>4</sub>, 30 NaHCO<sub>3</sub>, 20 HEPES, 2 MgCl<sub>2</sub>, 2 CaCl<sub>2</sub>, 25 glucose, 5 L(+)-

530 ascorbic acid, 2 thiourea, 3 Na-pyruvate (titrated to pH 7.2-7.3 with NaOH). In the recording  
531 chamber, slices were superfused with oxygenated standard artificial cerebrospinal fluid  
532 (aCSF) containing (in mM): 130 NaCl, 25 NaHCO<sub>3</sub>, 2.5 KCl, 1.25 NaH<sub>2</sub>PO<sub>4</sub>, 1.2 MgCl<sub>2</sub>, 2  
533 CaCl<sub>2</sub>, 18 glucose, 1.7 L(+)-ascorbic acid.

534 Whole-cell patch clamp recordings were performed at nearly physiological temperature (30-  
535 32°C), with borosilicate pipettes (3-4 MΩ) filled with (in mM): 130 KGlucuronate, 10 KCl, 10  
536 HEPES, 10 phosphocreatine, 0.2 EGTA, 4 Mg-ATP, 0.2 Na-GTP (290-300 mOsm, pH 7.2-  
537 7.3). A control experimental series was conducted with narrow pipettes tips (9-10 MΩ) filled  
538 with (in mM): 130 KGlucuronate, 5 KCl, 10 HEPES, 5 Sucrose (275-280 mOsm, pH 7.2-7.3),  
539 in order to delay intracellular dialysis(46) and minimize interference with intracellular ATP  
540 and Ca<sup>2+</sup> levels. In this series, neuronal firing was measured within the first 1.5 min after  
541 whole-cell establishment (supplementary figure 8).

542 To elicit neuronal firing, cells were held at -60 mV with direct current injections, and somatic  
543 current injections of increasing amplitude were provided using ramps of 5 s (6 ramps with  
544 final amplitude ranging from 50 pA to 300 pA) or squared pulses of 2 s (25 pA delta increase,  
545 max amplitude 200 pA). Input resistance (R<sub>i</sub>) was assessed by the passive current response to  
546 a -10 mV hyperpolarizing step while cells were held at -60 mV. In control condition, resting  
547 membrane potential (V<sub>rpm</sub>) and neuronal firing were measured within the first 5 min from the  
548 establishment of the whole-cell condition. The rheobase and the firing threshold were  
549 measured as the level of current and voltage, respectively, that induced the first action  
550 potential in the ramp protocol. The effect of β-hydroxybutyrate (2 mM) was assessed after  
551 >20 min perfusion, and compared to cell firing prior to perfusion.

552 Signals were acquired through a Digidata1550A digitizer, amplified through a Multiclamp  
553 700B amplifier, sampled at 20 kHz and filtered at 10 kHz using Clampex10 (Molecular  
554 Devices).

555

556 **Cell culture and lentiviral transduction**

557 Wild type pregnant mice were decapitated and E18 embryos were collected in HBSS medium.  
558 Primary cultures of cortical neurons were prepared as described previously(56). For MPC1  
559 downregulation, at 7 days in vitro (DIV), neurons were treated with lentiviral particles  
560 containing shRNA targeting MPC1 for a further 7-8 days. Briefly, to prepare viral particles,  
561 Hek293T cells were transfected with packaging and envelope expressing plasmids together  
562 with PLKO.1-shRNA control (SHC016, SIGMA) or targeting MPC1 (ShMPC1\_1:  
563 CCGGGCTGCCTTACAAGTATTAATCTCGAGATTTAATACTTGTAAGGCAGCTTTTT ; shMPC1\_2 :  
564 CCGGGCTGCCATCAATGATATGAAACTCGAGTTTCATATCATTGATGGCAGCTTTTT), and after 72  
565 hours the culture supernatant was collected, ultracentrifugated at 100,000 g for 2 hours.

566

567 **Determination of oxygen consumption rate (OCR) and extracellular acidification rate**  
568 **(ECAR)**

569 Measurement of oxygen consumption was performed using a Seahorse XF 24 extracellular  
570 flux analyzer (Seahorse Biosciences). 80' 000 cells were seeded in XF24 cell culture  
571 microplates and grown for 16 days. Measurement of basal and stimulation-dependent oxygen  
572 consumption was carried out at 37°C in aCSF (140 mM NaCl, 5 mM KCl, 1.2 mM KH<sub>2</sub>PO<sub>4</sub>,  
573 1.3 mM MgCl<sub>2</sub>, 1.8 mM CaCl<sub>2</sub>, 5 mM Glucose, and 15 mM HEPES, pH 7.4). Cells were  
574 infected with control shRNA or shMPC1 as described above or treated with MPC1 inhibitors  
575 Zaprinast(57), Rosiglitazone(19) , and UK5099(58) at 5, 5 and 1 µM, respectively. Cells were  
576 treated as indicated in the figure legends for 30 min before performing the assay. Basal  
577 oxygen consumption was measured before injection. At the times indicated, the following  
578 compounds were injected: oligomycin (1 µM), FCCP (4 µM), Rotenone/Antimycin A (1 µM).



579 Each measurement loop consisted of 30 sec mixing, 2 min incubation, and 3 min  
580 measurement of oxygen consumption.

581 Determination of the extracellular acidification was carried out under the same conditions but  
582 in the absence of HEPES. The basal acidification rate was measured before injection. At the  
583 times indicated, the following compounds were injected: oligomycin (1  $\mu$ M), 2-deoxyglucose  
584 (5 mM). Each measurement loop consisted of 2 min mixing, 2 min incubation, and 3 min  
585 measurement of oxygen consumption.

586

### 587 **ATP measurements**

588 ATP measurements were performed on 15-17 DIV neurons, infected with control or MPC1  
589 shRNA as described above, or treated 30 minutes prior to performing the assay with MPC  
590 inhibitors. Neurons were washed and scraped in PBS. Neurons were centrifugated at 1000  
591 rpm for 5 min and resuspended in 100 mL of CellTiter Glo reagent and agitated for 2 min to  
592 allow cell lysis. After 10 min incubation, luminescence was recorded.

593

### 594 **Calcium imaging**

595 E18.5 primary cortical neurons were isolated and seeded onto 35mm Fluorodishes. Neurons  
596 were treated with control or MPC1 shRNA at 7DIV and used for calcium imaging at 14-17  
597 DIV. Neurons were loaded with 5  $\mu$ M FuraFF or Fura2 (F14181 and F1221, Thermo Fisher  
598 Scientific) in recording buffer (150 mM NaCl, 4.25 mM KCl, 4 mM NaHCO<sub>3</sub>, 1.25 mM  
599 NaH<sub>2</sub>PO<sub>4</sub>, 1.2 mM CaCl<sub>2</sub>, 10 mM D-glucose, and 10 mM HEPES at pH 7.4) with 0.02%  
600 pluronic acid, at 37 °C and 5% CO<sub>2</sub> for 30 min.

601 After washing, the cells were imaged in recording buffer using a custom-made imaging  
602 widefield system built on an IX71 Olympus microscope equipped with a 20 $\times$  water objective.

603 A Xenon arc lamp with a monochromator was used for excitation, exciting FuraFF or Fura2

604 fluorescence alternately at 340 nm  $\pm$  20 nm and 380 nm  $\pm$  20 nm and collecting  
605 emitted light through a dichroic T510lpxru or a 79003-ET Fura2/TRITC (Chroma), and a  
606 band-pass filter 535/30 nm. Neurons were stimulated using 10  $\mu$ M glutamate (G1626,  
607 Sigma) and 10  $\mu$ M Ionomycin was added at the end of each time course experiment as a  
608 positive control. Images were acquired using a Zyla CMOS camera (Andor) every 2–5 s.  
609 The images were then analysed using ImageJ.

610 Briefly, Regions of Interest (ROIs) were selected and average fluorescence intensity was  
611 measured for each channel including the background fluorescence. After subtracting the  
612 background fluorescence, the ratio between 380 and 340 nm was calculated and plotted as  
613 cytosolic [Ca<sup>2+</sup>] levels upon stimulation. The Mean amplitude was calculated for each cell  
614 using Graphpad Prism.

615

### 616 **Statistical analysis**

617 The comparison of two groups was performed using a two-sided Student's t-test or its non  
618 parametric correspondent, the Mann-Whitney test, if normality was not granted either because  
619 not checked ( $n < 10$ ) or because rejected (D'Agostino and Pearson test). The comparisons of  
620 more than two groups were made using one or two ways ANOVAs followed by post-hoc  
621 tests, described in the figure legends, to identify all the significant group differences. N  
622 indicates independent biological replicates from distinct samples. Data are all represented as  
623 scatter or aligned dot plot with centre line as mean, except for western blot quantifications,  
624 which are represented as histogram bars. The graphs with error bars indicate 1 SEM (+/-) and  
625 the significance level is denoted as usual (\* $p < 0.05$ , \*\* $p < 0.01$ , \*\*\* $p < 0.001$ ). All the  
626 statistical analyses were performed using Prism7 (Graphpad version 7.0a, April 2, 2016).

627

628

629 **References**

630  
631  
632  
633  
634  
635  
636  
637  
638  
639  
640  
641  
642  
643  
644  
645  
646  
647  
648  
649  
650  
651  
652  
653  
654  
655  
656  
657  
658  
659  
660  
661  
662  
663  
664  
665  
666  
667  
668  
669  
670  
671  
672  
673  
674  
675  
676

1. D. Attwell, S. B. Laughlin, An energy budget for signaling in the grey matter of the brain. *J Cereb Blood Flow Metab* **21**, 1133-1145 (2001).
2. C. N. Hall, M. C. Klein-Flugge, C. Howarth, D. Attwell, Oxidative phosphorylation, not glycolysis, powers presynaptic and postsynaptic mechanisms underlying brain information processing. *J Neurosci* **32**, 8940-8951 (2012).
3. M. S. Goyal, M. Hawrylycz, J. A. Miller, A. Z. Snyder, M. E. Raichle, Aerobic glycolysis in the human brain is associated with development and neotenus gene expression. *Cell Metab* **19**, 49-57 (2014).
4. S. N. Vaishnavi *et al.*, Regional aerobic glycolysis in the human brain. *Proc Natl Acad Sci U S A* **107**, 17757-17762 (2010).
5. D. Zala *et al.*, Vesicular glycolysis provides on-board energy for fast axonal transport. *Cell* **152**, 479-491 (2013).
6. C. M. Diaz-Garcia *et al.*, Neuronal Stimulation Triggers Neuronal Glycolysis and Not Lactate Uptake. *Cell Metab* **26**, 361-374 e364 (2017).
7. G. Ashrafi, T. A. Ryan, Glucose metabolism in nerve terminals. *Curr Opin Neurobiol* **45**, 156-161 (2017).
8. L. Pellerin *et al.*, Activity-dependent regulation of energy metabolism by astrocytes: An update. *Glia* **55**, 1251-1262 (2007).
9. D. K. Bricker *et al.*, A mitochondrial pyruvate carrier required for pyruvate uptake in yeast, Drosophila, and humans. *Science* **337**, 96-100 (2012).
10. S. Herzig *et al.*, Identification and functional expression of the mitochondrial pyruvate carrier. *Science* **337**, 93-96 (2012).
11. P. A. Vigueira *et al.*, Mitochondrial pyruvate carrier 2 hypomorphism in mice leads to defects in glucose-stimulated insulin secretion. *Cell Rep* **7**, 2042-2053 (2014).
12. B. Vanderperre *et al.*, Embryonic Lethality of Mitochondrial Pyruvate Carrier 1 Deficient Mouse Can Be Rescued by a Ketogenic Diet. *PLoS Genet* **12**, e1006056 (2016).
13. K. Brockmann *et al.*, Autosomal dominant glut-1 deficiency syndrome and familial epilepsy. *Ann Neurol* **50**, 476-485 (2001).
14. M. Brivet *et al.*, Impaired mitochondrial pyruvate importation in a patient and a fetus at risk. *Mol Genet Metab* **78**, 186-192 (2003).
15. L. Oonthonpan, A. J. Rauckhorst, L. R. Gray, A. C. Boutron, E. B. Taylor, Two human patient mitochondrial pyruvate carrier mutations reveal distinct molecular mechanisms of dysfunction. *JCI Insight* **5**, (2019).
16. F. Diaz, H. Kotarsky, V. Fellman, C. T. Moraes, Mitochondrial disorders caused by mutations in respiratory chain assembly factors. *Semin Fetal Neonatal Med* **16**, 197-204 (2011).
17. H. Beck, Y. Yaari, Plasticity of intrinsic neuronal properties in CNS disorders. *Nat Rev Neurosci* **9**, 357-369 (2008).

- 677 18. A. S. Divakaruni *et al.*, Inhibition of the mitochondrial pyruvate  
678 carrier protects from excitotoxic neuronal death. *J Cell Biol* **216**, 1091-  
679 1105 (2017).
- 680 19. A. S. Divakaruni *et al.*, Thiazolidinediones are acute, specific  
681 inhibitors of the mitochondrial pyruvate carrier. *Proc Natl Acad Sci U S*  
682 *A* **110**, 5422-5427 (2013).
- 683 20. N. R. Sibson *et al.*, Stoichiometric coupling of brain glucose  
684 metabolism and glutamatergic neuronal activity. *Proc Natl Acad Sci U S*  
685 *A* **95**, 316-321 (1998).
- 686 21. X. Wang, C. Zhang, G. Szabo, Q. Q. Sun, Distribution of  
687 CaMKIIalpha expression in the brain in vivo, studied by CaMKIIalpha-  
688 GFP mice. *Brain Res* **1518**, 9-25 (2013).
- 689 22. A. Dhir, Pentylentetrazol (PTZ) kindling model of epilepsy. *Curr*  
690 *Protoc Neurosci* **Chapter 9**, Unit9 37 (2012).
- 691 23. J. Carroll, K. Martin-McGill, H. Cross, M. Hickson, A. Collinson,  
692 Outcome measurement and reporting in childhood epilepsy treated with  
693 ketogenic diet therapy: a scoping review protocol. *JBI Database*  
694 *System Rev Implement Rep* **17**, 633-639 (2019).
- 695 24. E. Wirrell, S. Eckert, L. Wong-Kisiel, E. Payne, K. Nickels,  
696 Ketogenic Diet Therapy in Infants: Efficacy and Tolerability. *Pediatr*  
697 *Neurol* **82**, 13-18 (2018).
- 698 25. H. C. Peters, H. Hu, O. Pongs, J. F. Storm, D. Isbrandt,  
699 Conditional transgenic suppression of M channels in mouse brain  
700 reveals functions in neuronal excitability, resonance and behavior. *Nat*  
701 *Neurosci* **8**, 51-60 (2005).
- 702 26. N. Gu, H. Hu, K. Vervaeke, J. F. Storm, SK (KCa2) channels do  
703 not control somatic excitability in CA1 pyramidal neurons but can be  
704 activated by dendritic excitatory synapses and regulate their impact. *J*  
705 *Neurophysiol* **100**, 2589-2604 (2008).
- 706 27. D. L. Greene, N. Hoshi, Modulation of Kv7 channels and  
707 excitability in the brain. *Cell Mol Life Sci* **74**, 495-508 (2017).
- 708 28. N. A. Singh *et al.*, Mouse models of human KCNQ2 and KCNQ3  
709 mutations for benign familial neonatal convulsions show seizures and  
710 neuronal plasticity without synaptic reorganization. *J Physiol* **586**, 3405-  
711 3423 (2008).
- 712 29. T. J. Jentsch, B. C. Schroeder, C. Kubisch, T. Friedrich, V. Stein,  
713 Pathophysiology of KCNQ channels: neonatal epilepsy and progressive  
714 deafness. *Epilepsia* **41**, 1068-1069 (2000).
- 715 30. V. Barrese, J. B. Stott, I. A. Greenwood, KCNQ-Encoded  
716 Potassium Channels as Therapeutic Targets. *Annu Rev Pharmacol*  
717 *Toxicol* **58**, 625-648 (2018).
- 718 31. H. Hu, K. Vervaeke, J. F. Storm, M-channels (Kv7/KCNQ  
719 channels) that regulate synaptic integration, excitability, and spike  
720 pattern of CA1 pyramidal cells are located in the perisomatic region. *J*  
721 *Neurosci* **27**, 1853-1867 (2007).
- 722 32. R. W. Manville, M. Papanikolaou, G. W. Abbott, M-Channel  
723 Activation Contributes to the Anticonvulsant Action of the Ketone Body  
724 beta-Hydroxybutyrate. *J Pharmacol Exp Ther* **372**, 148-156 (2020).
- 725 33. A. Alaimo, A. Villarroel, Calmodulin: A Multitasking Protein in  
726 Kv7.2 Potassium Channel Functions. *Biomolecules* **8**, (2018).

- 727  
728  
729  
730  
731  
732  
733  
734  
735  
736  
737  
738  
739  
740  
741  
742  
743  
744  
745  
746  
747  
748  
749  
750  
751  
752  
753  
754  
755  
756  
757  
758  
759  
760  
761  
762  
763  
764  
765  
766  
767  
768  
769  
770  
771  
772  
773  
774  
775
34. N. Gamper, M. S. Shapiro, Calmodulin mediates Ca<sup>2+</sup>-dependent modulation of M-type K<sup>+</sup> channels. *J Gen Physiol* **122**, 17-31 (2003).
35. M. Shahidullah, L. C. Santarelli, H. Wen, I. B. Levitan, Expression of a calmodulin-binding KCNQ2 potassium channel fragment modulates neuronal M-current and membrane excitability. *Proc Natl Acad Sci U S A* **102**, 16454-16459 (2005).
36. X. Zhou *et al.*, Calmodulin regulates KCNQ2 function in epilepsy. *Am J Transl Res* **8**, 5610-5618 (2016).
37. A. Kosenko, N. Hoshi, A change in configuration of the calmodulin-KCNQ channel complex underlies Ca<sup>2+</sup>-dependent modulation of KCNQ channel activity. *PLoS One* **8**, e82290 (2013).
38. C. Giorgi *et al.*, Mitochondrial calcium homeostasis as potential target for mitochondrial medicine. *Mitochondrion* **12**, 77-85 (2012).
39. N. Nemani *et al.*, Mitochondrial pyruvate and fatty acid flux modulate MICU1-dependent control of MCU activity. *Sci Signal* **13**, (2020).
40. A. Grenell *et al.*, Loss of MPC1 reprograms retinal metabolism to impair visual function. *Proc Natl Acad Sci U S A* **116**, 3530-3535 (2019).
41. M. I. Cordero, N. Just, G. L. Poirier, C. Sandi, Effects of paternal and peripubertal stress on aggression, anxiety, and metabolic alterations in the lateral septum. *Eur Neuropsychopharmacol* **26**, 357-367 (2016).
42. K. Timper *et al.*, Mild Impairment of Mitochondrial OXPHOS Promotes Fatty Acid Utilization in POMC Neurons and Improves Glucose Homeostasis in Obesity. *Cell Rep* **25**, 383-397 e310 (2018).
43. P. Schonfeld, G. Reiser, Why does brain metabolism not favor burning of fatty acids to provide energy? Reflections on disadvantages of the use of free fatty acids as fuel for brain. *J Cereb Blood Flow Metab* **33**, 1493-1499 (2013).
44. P. Machler *et al.*, In Vivo Evidence for a Lactate Gradient from Astrocytes to Neurons. *Cell Metab* **23**, 94-102 (2016).
45. S. Jang *et al.*, Glycolytic Enzymes Localize to Synapses under Energy Stress to Support Synaptic Function. *Neuron* **90**, 278-291 (2016).
46. V. Jakkamsetti *et al.*, Brain metabolism modulates neuronal excitability in a mouse model of pyruvate dehydrogenase deficiency. *Sci Transl Med* **11**, (2019).
47. H. S. Wang *et al.*, KCNQ2 and KCNQ3 potassium channel subunits: molecular correlates of the M-channel. *Science* **282**, 1890-1893 (1998).
48. C. Biervert *et al.*, A potassium channel mutation in neonatal human epilepsy. *Science* **279**, 403-406 (1998).
49. B. C. Schroeder, C. Kubisch, V. Stein, T. J. Jentsch, Moderate loss of function of cyclic-AMP-modulated KCNQ2/KCNQ3 K<sup>+</sup> channels causes epilepsy. *Nature* **396**, 687-690 (1998).
50. H. Watanabe *et al.*, Disruption of the epilepsy KCNQ2 gene results in neural hyperexcitability. *J Neurochem* **75**, 28-33 (2000).

- 776 51. M. Campanella, N. Parker, C. H. Tan, A. M. Hall, M. R. Duchon,  
777 IF(1): setting the pace of the F(1)F(o)-ATP synthase. *Trends Biochem*  
778 *Sci* **34**, 343-350 (2009).  
779 52. E. Gebara *et al.*, Heterogeneity of Radial Glia-Like Cells in the  
780 Adult Hippocampus. *Stem Cells* **34**, 997-1010 (2016).  
781 53. C. B. Mishra *et al.*, The anti-epileptogenic and cognition  
782 enhancing effect of novel 1-[4-(4-benzo [1, 3] dioxol-5-ylmethyl-  
783 piperazin-1-yl)-phenyl]-3-phenyl-urea (BPPU) in pentylenetetrazole  
784 induced chronic rat model of epilepsy. *Biomed Pharmacother* **105**, 470-  
785 480 (2018).  
786 54. P. Megevand, C. Quairiaux, A. M. Lascano, J. Z. Kiss, C. M.  
787 Michel, A mouse model for studying large-scale neuronal networks  
788 using EEG mapping techniques. *Neuroimage* **42**, 591-602 (2008).  
789 55. L. Sheybani *et al.*, Electrophysiological Evidence for the  
790 Development of a Self-Sustained Large-Scale Epileptic Network in the  
791 Kainate Mouse Model of Temporal Lobe Epilepsy. *J Neurosci* **38**, 3776-  
792 3791 (2018).  
793 56. J. Faure *et al.*, Exosomes are released by cultured cortical  
794 neurones. *Mol Cell Neurosci* **31**, 642-648 (2006).  
795 57. J. Du *et al.*, Inhibition of mitochondrial pyruvate transport by  
796 zaprinast causes massive accumulation of aspartate at the expense of  
797 glutamate in the retina. *J Biol Chem* **288**, 36129-36140 (2013).  
798 58. A. P. Halestrap, The mitochondrial pyruvate carrier. Kinetics and  
799 specificity for substrates and inhibitors. *Biochem J* **148**, 85-96 (1975).  
800  
801

## 802 **Acknowledgments**

803 We would like express our sincere thanks to Drs. Nika Danial, Timothy Ryan, Garry Yellen  
804 and all members of the Martinou lab for helpful scientific discussion during the course of this  
805 work. We also wish to extend our special thanks to Dr. Fabien Lanté and Dr. Anita Lüthi for  
806 advices on the electrophysiology experiments, Dr. Kinsey Maundrell for help in reviewing the  
807 manuscript, to Professor Nicolas Toni (University of Lausanne) who kindly provided us the  
808 GFAP-CreERT2 mouse, to Professor Ivan Rodriguez (University of Geneva) who kindly  
809 provided us with the Ai14 reporter mouse.

810

## 811 **Author contributions**

812 JCM and ADLR conceived the project. ADLR performed and/or participated in all the *in-vivo*  
813 experiments, and analysed the data. ML designed, performed and analysed all experiments  
814 involving neuronal primary cultures and synaptosomes. SA designed, performed and analysed  
815 the electrophysiology experiments, under the supervision of CS. TM and AC performed the  
816 experiments using calcium imaging. ERF designed and performed behavioural analysis, under  
817 the supervision of CS. SM performed mouse breeding and genotyping and participated in  
818 some in vivo experiments. PS performed some of the calcium imaging experiment on cultured  
819 neurones, under the supervision of MD. AK and CQ performed EEGs. ET and JRu provided  
820 the MPC1 Flox/Flox mice and advices. JMN supervised statistical analysis. JCM, ADLR, ML  
821 and SA wrote the manuscript with input from all other authors.

822

## 823 **Funding agencies**

824 Swiss National Science Foundation [31003A\_179421/1 /1 and The Kristian Gerhard Jebsen  
825 Foundation to J.-C.M; Requip support from the Swiss National Science Fondation for the  
826 acquisition of the Seahorse apparatus (SNF 316030\_145001). Spanish Ministerio de

827 Economía y Competitividad (MINECO, BFU2017-84490-P and RYC-2015-18545) to PM.

828 **Conflict of interest statement.** None declared.

829

### 830 **Data availability**

831 The data that are supporting the findings of this study are available from the corresponding  
832 authors upon request .

833

### 834 **Figure legends**

835 **Figure 1. MPC-deficient neurons display defects in mitochondrial respiration and**

836 **membrane potential. A)** Profile and quantification of oxygen consumption rates (OCR)

837 cortical neurons expressing either shCtrl, or shMPC1\_1 and shMPC1\_2 for 7 days, or in the  
838 presence of Zaprinast (5 $\mu$ M, 1 hour). Data were obtained using the Seahorse XF analyzer.

839 Assays were performed in the presence of pyruvate (5 mM) and glucose (5 mM) as carbon  
840 sources. Quantification of basal OCR is expressed as ratio of ShCtrl. N=10,7,9,7 and 2

841 independent experiments. N=33,11,25 and 6 independent experiments. One-way

842 ANOVA+Tukey's post-hoc test (shCtrl vs Zaprinast p=0.0001, shCtrl vs shMPC1\_1

843 p=0.0001, shCtrl vs shMPC1\_2 p=0.0013). **B)** ATP content in MPC-deficient cortical neurons

844 treated with either shCtrl, Zaprinast or shMPC1\_1 and shMPC1\_2. FCCP (4  $\mu$ M) treatment

845 reveals the non-mitochondrial ATP. N=10,7,9,7 and 2 independent experiments. One-way

846 ANOVA+Tukey's post-hoc test (shCtrl vs Zaprinast p=0.0006, shCtrl vs shMPC1\_1

847 p=0.0223, shCtrl vs shMPC1\_2 p=0.0242, shCtrl vs FCCP p=0.0001). **C)** Mitochondrial

848 membrane potential of MPC-deficient cortical neurons. Neurons were incubated with

849 Mitotracker red (MtR) (1  $\mu$ M) prior fixation, immunostained for  $\beta$ III tubulin (neuron) and

850 TOM20 (mitochondria). Quantification of Mitotracker red fluorescence in each  $\beta$ III tubulin-

851 positive cell (red) was reported to TOM20 signal (green). N=15 neurons from 3 independent



852 experiments. Unpaired t test (shCtrl vs shMPC1  $p=0.0001$ ). **D)** Profile and quantification of  
853 oxygen consumption rates (OCR) in cortical neurons expressing shCtrl or shMPC1\_1 for 7  
854 days. Data were obtained using the Seahorse XF analyzer. Assays were performed in the  
855 presence of pyruvate (5 mM) and glucose (5 mM) as carbon sources + 10 mM  $\beta$ HB when  
856 indicated. Quantification of basal OCR is expressed as ratio of control condition shCtrl. N=12  
857 independent experiment. One-way ANOVA+Holm Sidak's post-hoc test (shCtrl vs shMPC1  
858  $p=0.0001$ , shMPC1 vs shMPC1+ $\beta$ HB  $p=0.0002$ ). **E)** ATP content in MPC-deficient cortical  
859 neurons treated with shCtrl or shMPC1 in presence or absence of 10 mM  $\beta$ HB. FCCP (4  $\mu$ M)  
860 treatment reveals the non-mitochondrial ATP. N=10, 9, 10, 9 independent experiments. One-  
861 way ANOVA+Holm Sidak's post-hoc test (shCtrl vs shMPC1  $p=0.0145$ , shMPC1 vs  
862 shMPC1+ $\beta$ HB  $p=0.0143$ , shCtrl vs FCCP  $p=0.0001$ ). **F)** Cortical neurons were incubated  
863 with TMRE (50 nM) +/-  $\beta$ HB (10 mM) for 30 min and recorded by live microscopy. Neurons  
864 were incubated with DMSO or Zaprinast (5  $\mu$ M) 2.5 min after the beginning of the  
865 acquisition and recorded for 5 min prior FCCP injection. N=15 independent experiments.  
866 One-way ANOVA+Holm Sidak's post-hoc test (shCtrl vs Zaprinast  $p=0.0028$ , Zaprinast vs  
867 Zaprinast+ $\beta$ HB  $p=0.0008$ ).

868

869 **Figure 2. Generation of mice with an inducible deletion of the MPC1 gene in adult**  
870 **glutamatergic neurons.** **A)** Strategies used to generate CamKII $\alpha$ -Cre<sub>ERT2</sub>/MPC1<sup>Flox</sup> mice.  
871 Upon Tamoxifen injection, expression of the Cre recombinase in CamKII $\alpha$  glutamatergic  
872 neurons drives deletion of the MPC1 gene. These mice are referred to as neuro-MPC1-KO or  
873 neuro-MPC1-WT when they are CamCre- (1. Glutamatergic neuron; 2. Astrocytes; 3.  
874 Inhibitory neuron). **B)** Immunostaining of MPC1 (red) in cortical sections from neuro-MPC1-  
875 WT and neuro-MPC1-KO mice (scale bar: 100  $\mu$ m). **C)** Western blot analysis of whole  
876 cortex, synaptosome lysates and heavy organelles (mainly mitochondria), obtained from

877 brains of neuro-MPC1-WT and neuro-MPC1-KO mice using neuronal (Synaptophysin,  
878 tyrosine hydroxylase, CamKII $\alpha$ ) and astroglial markers (GFAP) as well as mitochondrial  
879 markers (MPC1, MPC2 and VDAC). Note that synaptosomes are enriched for CamKII $\alpha$ , a  
880 marker of excitatory neurons. Quantification (right panel) shows that except for MPC1 and  
881 MPC2, the content of these markers is similar in WT and KO preparations. N=6 independent  
882 neuro-MPC1-WT and neuro-MPC1-KO mice. Mann-Whitney test ((6) neuro-MPC1-WT vs  
883 neuro-MPC1-KO p=0.0286, (7) neuro-MPC1-WT vs neuro-MPC1-KO p=0.0152).

884

885 **Figure 3. Neuro-MPC1-KO mice are highly sensitive to pro-convulsant drugs and**  
886 **develop acute epileptic-like seizures. A)** Schematic description of the PTZ kindling  
887 protocol. **B)** Seizure severity scores reflecting the different clinical symptoms as indicated,  
888 obtained for neuro-MPC1-WT or neuro-MPC1-KO. N=8 independent neuro-MPC1-WT and  
889 neuro-MPC1-KO mice. Two way ANOVA (F(7,70)=19, p=0.0001). **C)** Illustration of the  
890 recording setups in awake mice indicating the position of surface EEG electrodes and  
891 representative example of a seizure recorded in a neuro-MPC1-KO mouse after injection of  
892 35mg/kg PTZ during surface EEG recordings. The inset shows an example of fast ripples  
893 generated during an ictal epileptic discharge. **D-I)** GCaMP6S calcium imaging of the CA1  
894 area from hippocampal slices in the presence of Carbachol (50 $\mu$ M) and PTZ (2mM). Slices  
895 were prepared from WT animals (top, black) or from KO animals with no pre-treatment  
896 (bottom, red). **D)** Ca<sup>2+</sup> sweeps recorded in four representative GCaMP6S-expressing neurons.  
897 **E)** Raster plots of Ca<sup>2+</sup> transient onsets extracted from all recorded neurons in a given slice.  
898 **F)** Cumulative distribution of the frequency of the calcium events in all the recorded neurons.  
899 N=7, 12 independent experiments. Kolmogorov-Smirnov test (WT vs KO p=0.0001). **G)**  
900 Cumulative distribution of the occurrence of neuronal co-activations exceeding chance levels  
901 as a function of time N=7, 12 independent experiments. Kolmogorov-Smirnov test (WT vs

902 KO  $p=0.0344$ ). Amplitude (**H**), and duration (**I**) of the calcium events recorded in all neurons  
903 of the hippocampus.  $N=7$ , 12 independent experiments. Mann-Whitney test (Amplitude: WT  
904 vs KO  $p=0.5918$ ; Duration: WT vs KO  $p=0.9182$ ).

905

906 **Figure 4. Ketogenic diet prevents the epileptic phenotype of neuro-MPC1-KO mice. A)**

907 Effect of the ketogenic diet (KD) on PTZ-induced seizure. All neuro-MPC1-KO mice were  
908 maintained on the Standard (SD) or ketogenic (KD) diet for 7 days prior to challenge with a  
909 single dose of PTZ. Clinical scores were assessed directly following injection.  $N=7$   
910 independent neuro-MPC1-KO mice. Mann-Whitney (neuro-MPC1-KO SD vs neuro-MPC1-  
911 KO KD  $p=0.0008$ ). **B)** Effects 1%  $\beta$ HB in the drinking water for 7 days, overnight fasting or  
912 ip injection of  $\beta$ HB 15 min before administration of PTZ into neuro-MPC1-KO mice.  $N=4$   
913 independent neuro-MPC1-KO mice. One-way ANOVA+Holm Sidak's post-hoc test (Vehicle  
914 vs all conditions  $p=0.0001$ ). **C)** Effect of  $\beta$ HB on PTZ-induced seizure: mice were injected ip  
915 with 1g/kg  $\beta$ HB, 15 minutes before each PTZ injection and scored for clinical symptoms.  
916  $N=6$  independent mice. Two-way ANOVA+Holm Sidak's post-hoc test ( $F(10, 75)=8$ , Neuro-  
917 MPC1-WT vs neuro-MPC1-KO, neuro-MPC1-KO vs neuro-MPC1-KO +  $\beta$ HB  $p=0.0001$ ).

918

919 **Figure 5. MPC1 deletion increases intrinsic excitability in CA1 pyramidal cells. A)**

920 Example voltage responses elicited in CA1 pyramidal cells from wild-type (WT) and MPC1-  
921 CamKII-KO (KO) by injection of current ramps (protocol at the bottom, only three of six  
922 ramps displayed). **B)** Frequency-current (F-I) relationship of action potential discharges,  
923 indicating higher spiking frequency in KO cells (Two-way ANOVA,  $F(1, 156) 33.43$ ,  
924  $p<0.0001$ ). **C)** The rheobase was reduced in KO cells (Mann-Whitney test,  $U=53.5$ ,  
925  $p=0.0406$ ). **D)** KO cells exhibited more hyperpolarized threshold potential (unpaired t test,  
926  $t=2.856$ ,  $p=0.0084$ ). **E)** Example traces showing lack of changes in WT cell firing after bath

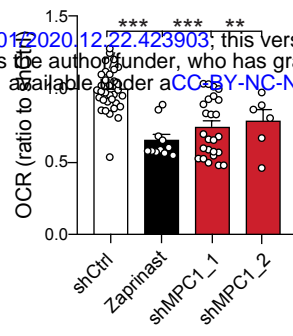
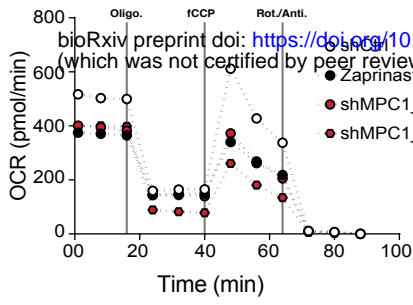
927 application of the ketone body  $\beta$ -hydroxybutyrate ( $\beta$ HB, 2 mM, >20 min exposure). **F)**  
928 Average firing frequency elicited by the 3<sup>rd</sup> ramp of current injections in WT cells in control  
929 condition (5 min after whole-cell establishment) and after 20 min of either no drug exposure  
930 or  $\beta$ HB application (no drug: paired t test,  $t=0.664$ ,  $p=0.5362$ ;  $\beta$ HB: paired t test,  $t=2.1$ ,  
931  $p=0.0804$ ). **G, H)** Example traces and summary graphs indicating significant reduction in KO  
932 cell firing after  $\beta$ HB application (no drug: paired t test,  $t=0.4691$ ,  $p=0.6634$ ;  $\beta$ HB: paired t  
933 test,  $t=5.339$ ,  $p=0.0005$ ). **I)** Example traces of cell firing in control and after bath application  
934 of XE991 (10  $\mu$ M) in WT and KO neurons. **J)** Average firing frequency elicited by the 2<sup>nd</sup>  
935 ramp of current injections in control and after XE991 application, indicating increased  
936 excitability in WT cells (paired t test,  $t=3.735$ ,  $p=0.0057$ ). XE991 was ineffective in KO cells,  
937 in which subsequent application of  $\beta$ HB also failed to modulate excitability (One-way  
938 ANOVA,  $F(1.69, 11.89)=4.76$ ,  $p=0.0347$ , Holm-Sidak's multiple comparison  $p>0.05$ ). **K)**  
939 XE991 significantly reduced the rheobase of WT cells (paired t test,  $t=11$ ,  $p<0.001$ ), but not  
940 of KO cells, in which subsequent  $\beta$ HB application was also ineffective (One-way ANOVA,  
941  $F(1.785, 12.5)=2.99$ ,  $p=0.091$ ). **L)** XE991 induced a shift in the threshold potential of WT  
942 cells (paired t test,  $t=6.001$ ,  $p=0.0003$ ), but did not affect KO cells, in which subsequent  $\beta$ HB  
943 application was also ineffective (One-way ANOVA,  $F(1.812, 12.68)=1.78$ ,  $p=0.209$ ). **M)**  
944 Example traces of KO cell firing elicited by a current ramp (300 pA max amplitude, APs are  
945 trimmed) in control and after  $\beta$ HB exposure, with expanded portion at the bottom indicating  
946 mAHP measurement. **N)** Summary graph of mAHP values in WT and KO cells in control and  
947 after  $\beta$ HB exposure, indicating significant increase in KO (unpaired t test,  $t=2.89$ ,  $p=0.0179$ ).  
948 **O)** Example traces of KO cell firing before and after application of retigabine (10  $\mu$ M), and  
949 subsequent  $\beta$ HB superfusion (2 mM). **P)** F-I relationships in KO cells, indicating reduced  
950 spiking frequency after retigabine application, with no additional effect of  $\beta$ HB (Two-way  
951 repeated measures ANOVA,  $F(2, 48)=89.15$ ,  $p<0.0001$ ).

952

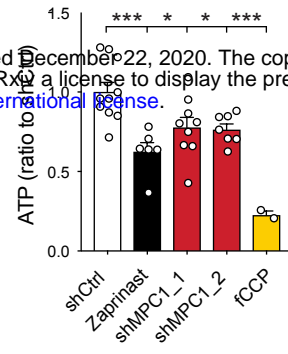
953 **Figure 6. Defect in calcium homeostasis.** **A)** Mean fluorescence signal intensity of cortical  
954 neurons loaded with furaFF-AM stimulated with 10  $\mu$ M glutamate (dashed black arrow) prior  
955 the addition of ionomycin (red arrow) to reveal the neuronal calcium stock. **B, C)** Graph  
956 showing the quantifications of control neurons, MPC-depleted neurons and MPC-depleted  
957 neurons+ $\beta$ HB showing an elevated level of cytosolic calcium in MPC-deficient stimulated  
958 neurons measured by FuraFF-AM (**B**) or Fura2-AM (**C**).  $N > 15$  neurons per condition from 3  
959 independent experiments. One-way ANOVA+Holm Sidak's post-hoc test ((**B**) shCtrl vs  
960 shMPC1  $p = 0.0286$ , shMPC1 vs shMPC1+ $\beta$ HB  $p = 0.0001$ ; (**C**) shCtrl vs shMPC1  $p = 0.0169$ ,  
961 shMPC1 vs shMPC1+ $\beta$ HB  $p = 0.0001$ ). **D)** Fluorescence signal intensity of control, MPC-  
962 deficient, and RU360-treated cortical neurons permeabilized with pluronic acid (0.02%).  
963 Neurons were loaded with Fura2-AM, stimulated with KCl 50 mM prior addition of fCCP to  
964 reveal the mitochondrial stocks of calcium. **E, F)** Quantification of calcium increased upon  
965 depolarization (**E**, ratio of the fluorescence peak after adding KCl to the mean of the 10 first  
966 basal measurement) and the amount of mitochondrial calcium released by fCCP (**F**, ratio of  
967 the fluorescence peak after adding fCCP to the lowest point during wash) in normal, MPC-  
968 deficient neurons and neurons+RU360.  $N > 13$  neurons per condition from 3 independent  
969 experiments. One-way ANOVA+Holm Sidak's post-hoc test ((**E**) Ctrl vs Zaprinast  
970  $p = 0.0389$ , Ctrl vs UK-5099  $p = 0.0054$ , Ctrl vs Rosiglitazone  $p = 0.0001$ , Ctrl vs RU360  
971  $p = 0.0001$ ; (**F**) Ctrl vs all conditions  $p = 0.0001$ ). **G, H)** Example traces and F-I relationship in  
972 WT cells with standard intracellular solution and with a solution containing the MCU  
973 inhibitor RU360 (1 or 10  $\mu$ M), which increased neuronal firing (10  $\mu$ M: Two-way ANOVA,  
974  $F(1, 72) = 26.03$ ,  $p < 0.0001$ ). **I, J)** Lack of RU360 (10  $\mu$ M) effect on neuronal firing in KO  
975 cells (Two-way ANOVA,  $F(1, 72) = 0.03607$ ,  $p = 0.8499$ ). **K)** Example traces of WT cell  
976 firing elicited by a current ramp (300 pA max amplitude, APs are trimmed) in control

977 condition and with RU360, with expanded portion at the bottom indicating mAHP  
978 measurement. **L)** Summary graph of mAHP values in control condition and with RU360,  
979 indicating significant reduction in WT (unpaired t test,  $t = 2.352$ ,  $p = 0.0392$ ). **M, N)** Example  
980 traces and F-I relationship in WT cells infused with RU360 (10  $\mu$ M) and subsequently  
981 exposed to  $\beta$ HB (2 mM, >20 min exposure), which decreased neuronal firing (Two-way  
982 ANOVA,  $F(1, 28) = 17.69$ ,  $p = 0.0001$ ) and augmented mAHP (inset, paired t test,  $t = 2.336$ ,  
983  $p = 0.0477$ ).  
984

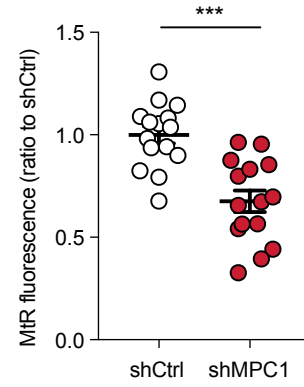
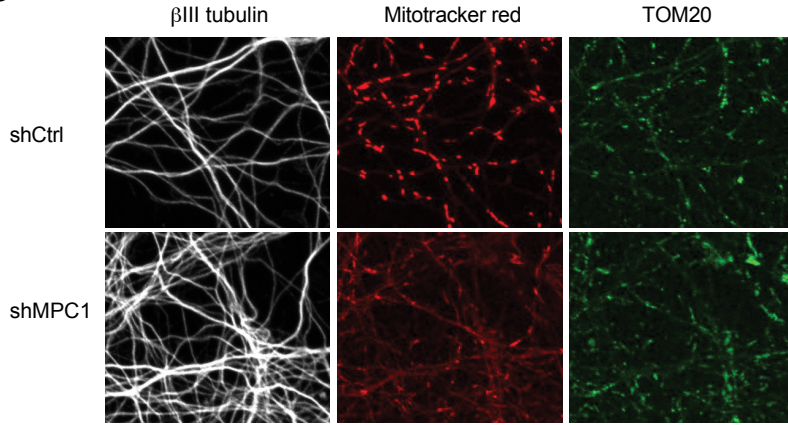
A



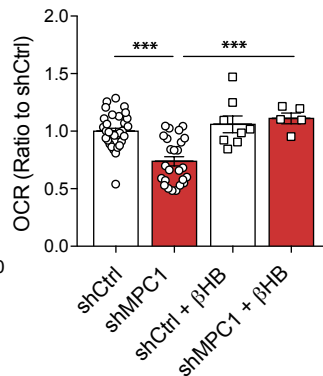
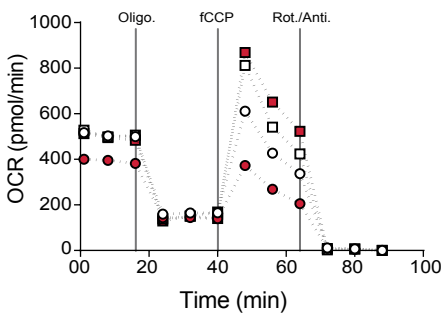
B



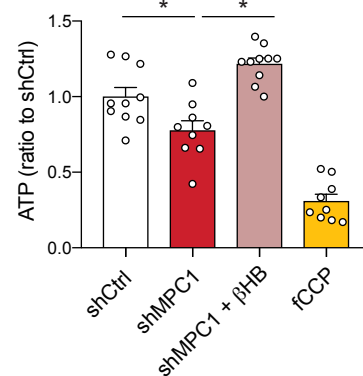
C



D



E



F

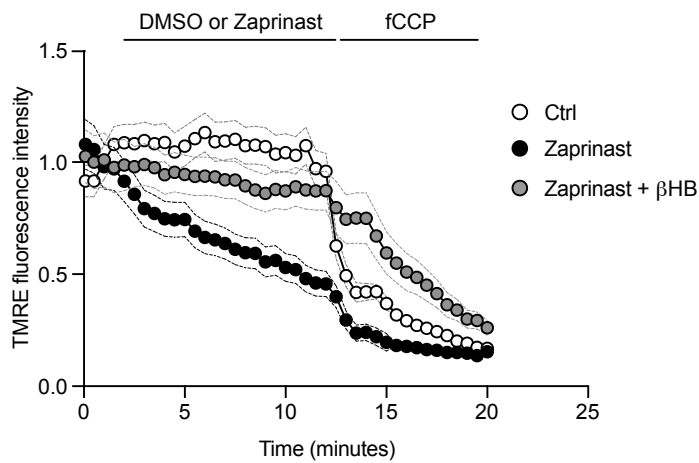
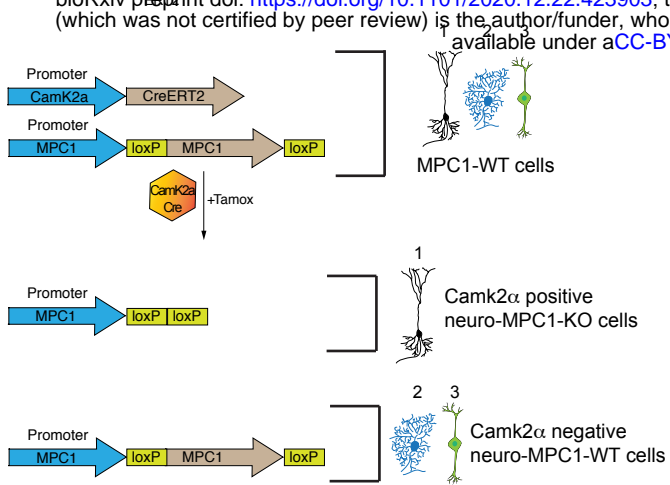
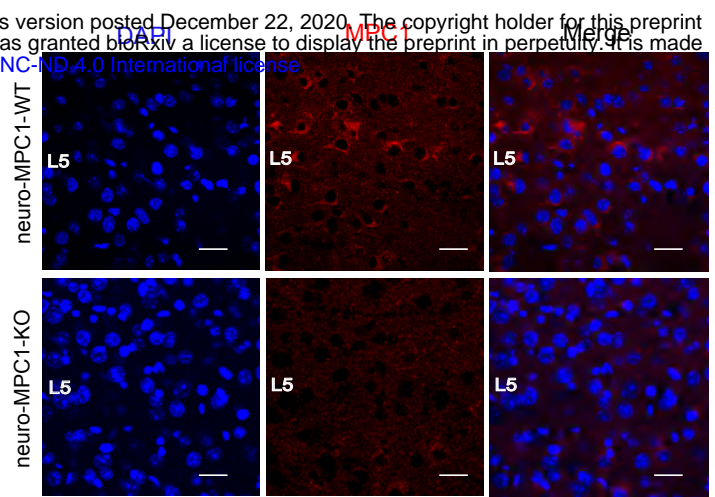


Figure 1

A

Camk2 $\alpha$ -Cre<sup>+</sup>/MPC1<sup>Flox</sup> Mice

B



C

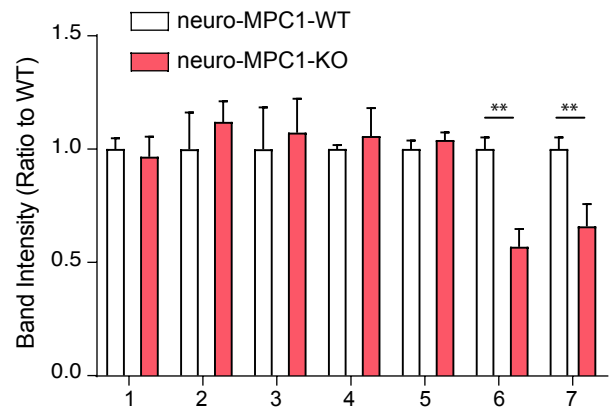
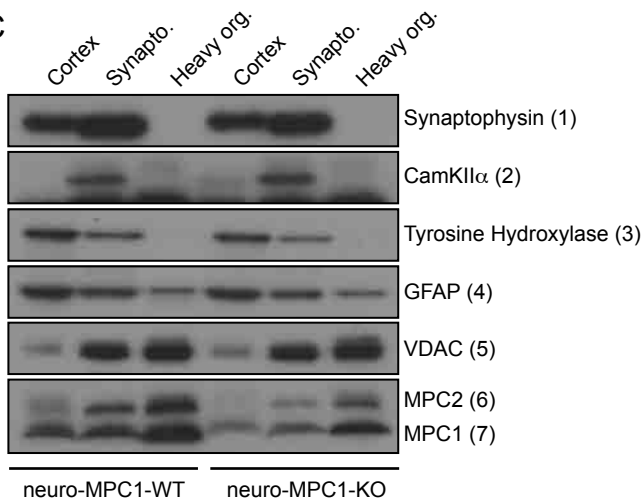


Figure 2



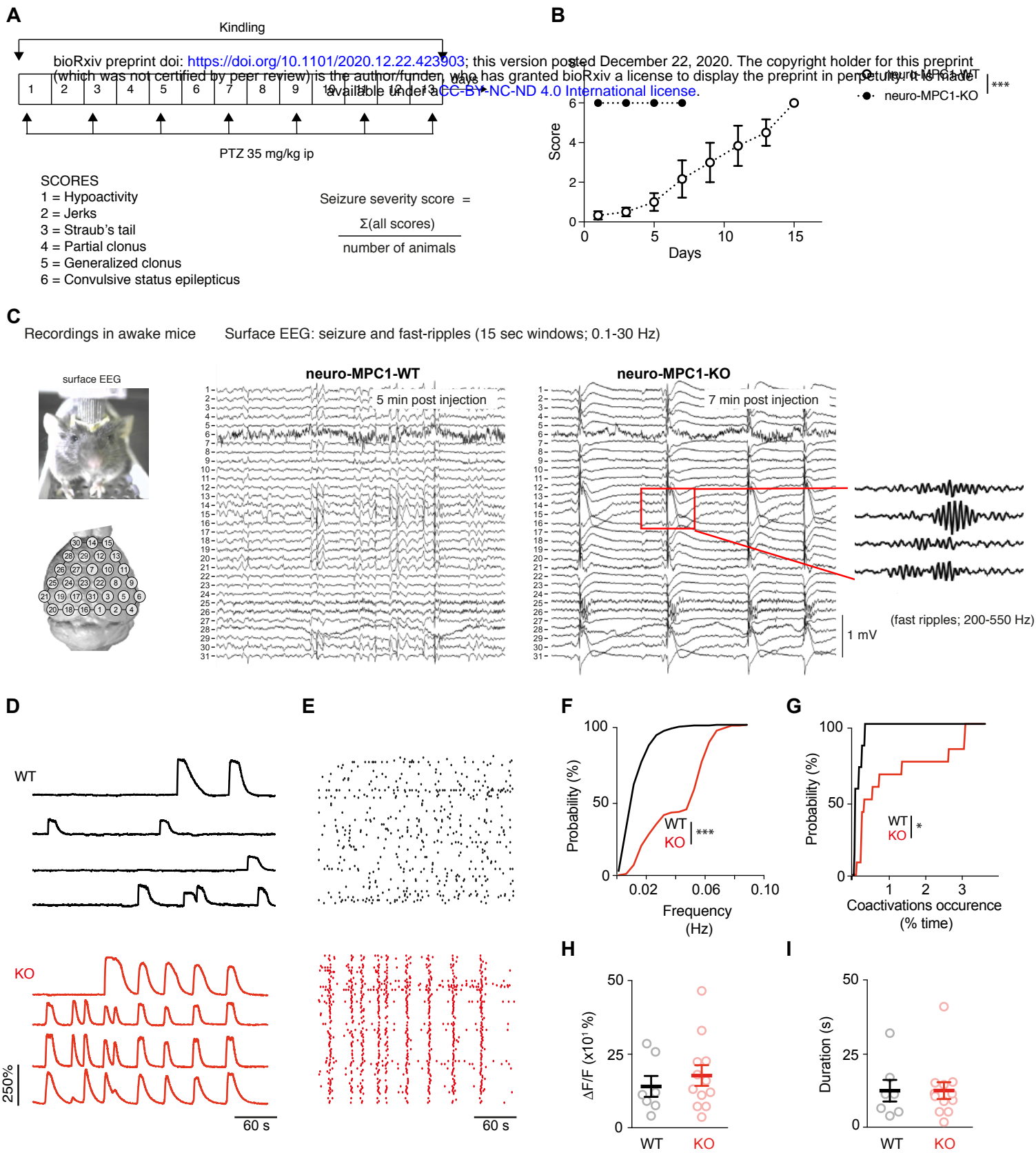


Figure 3

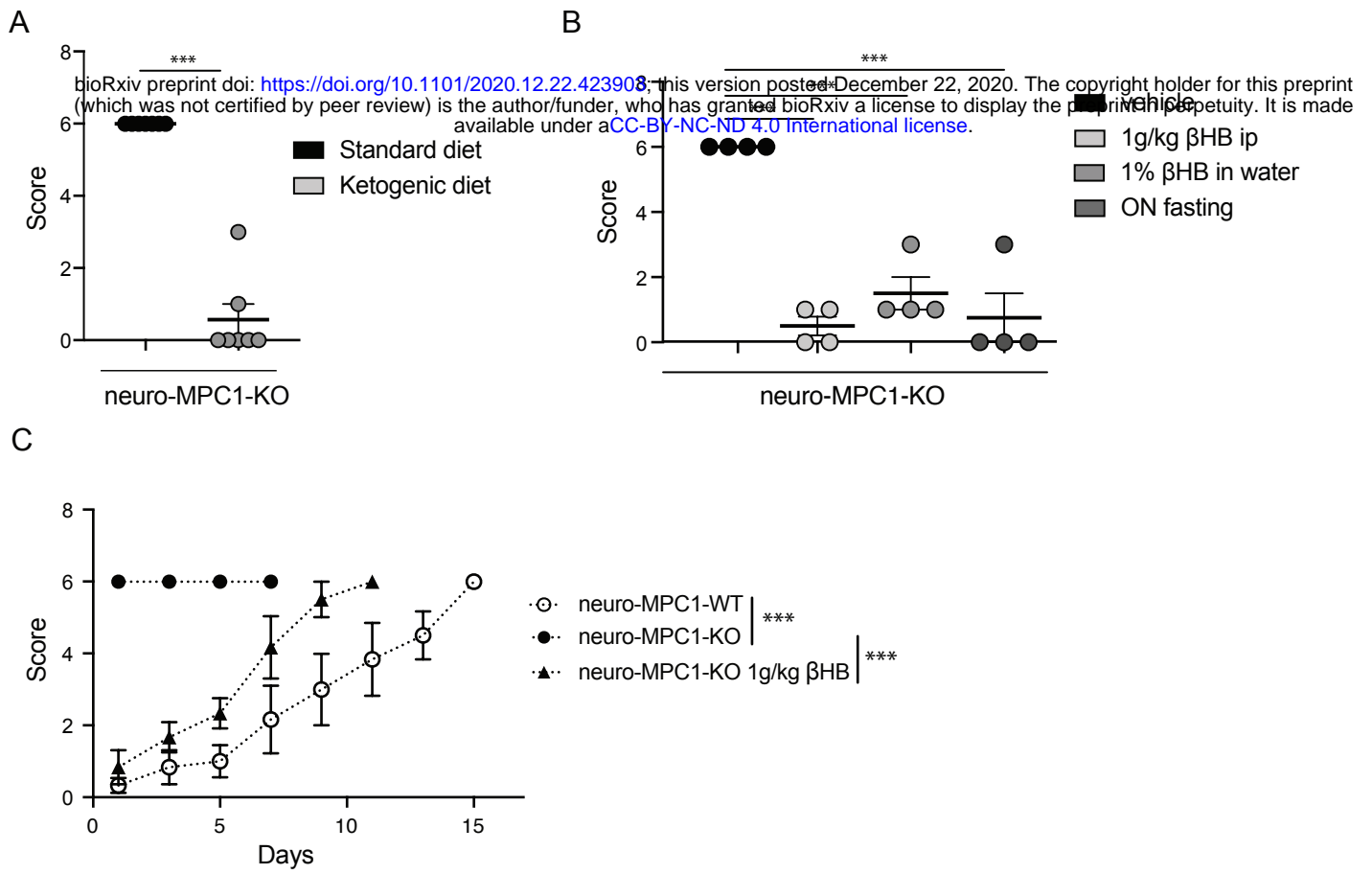


Figure 4

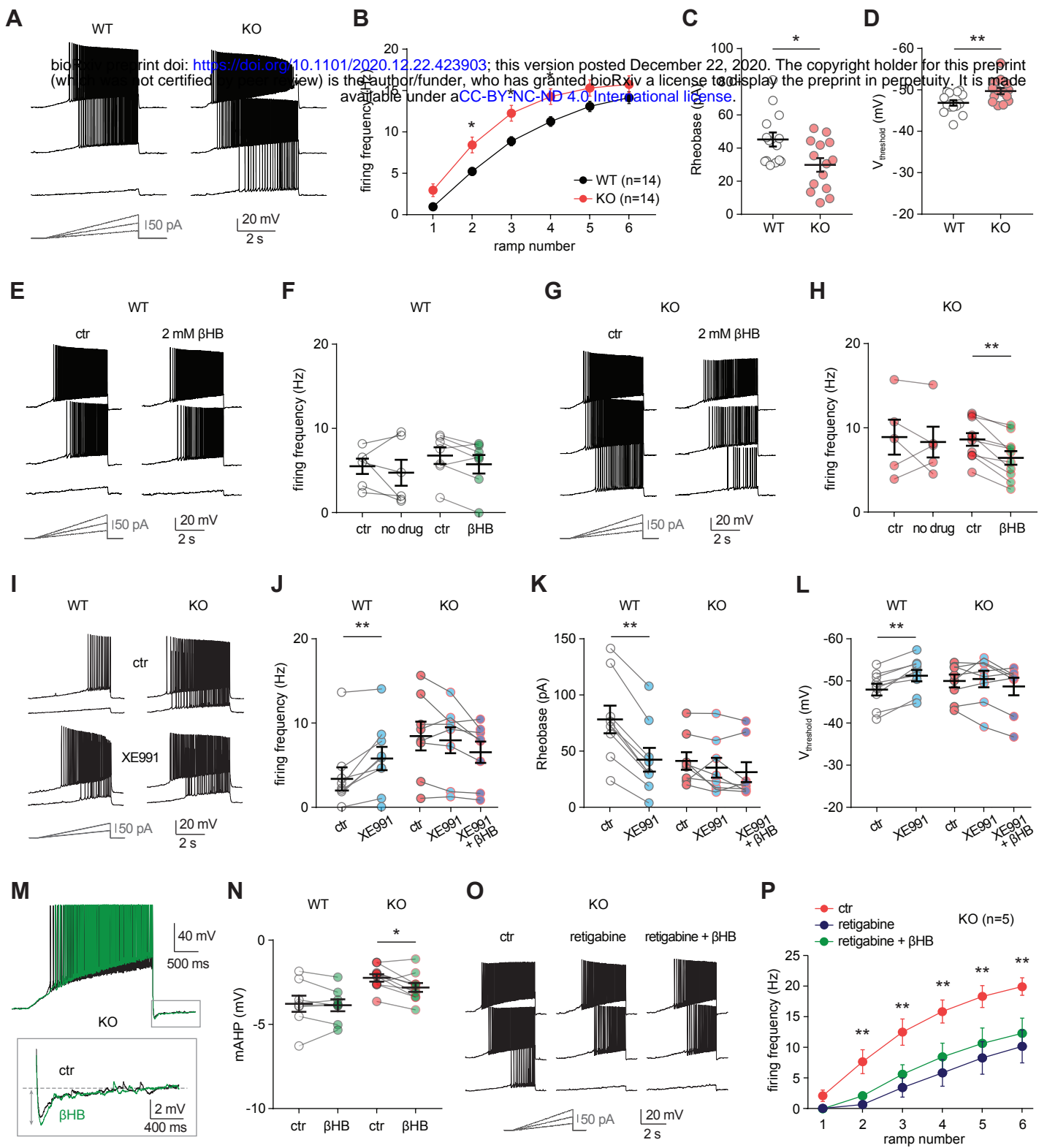


Figure 5

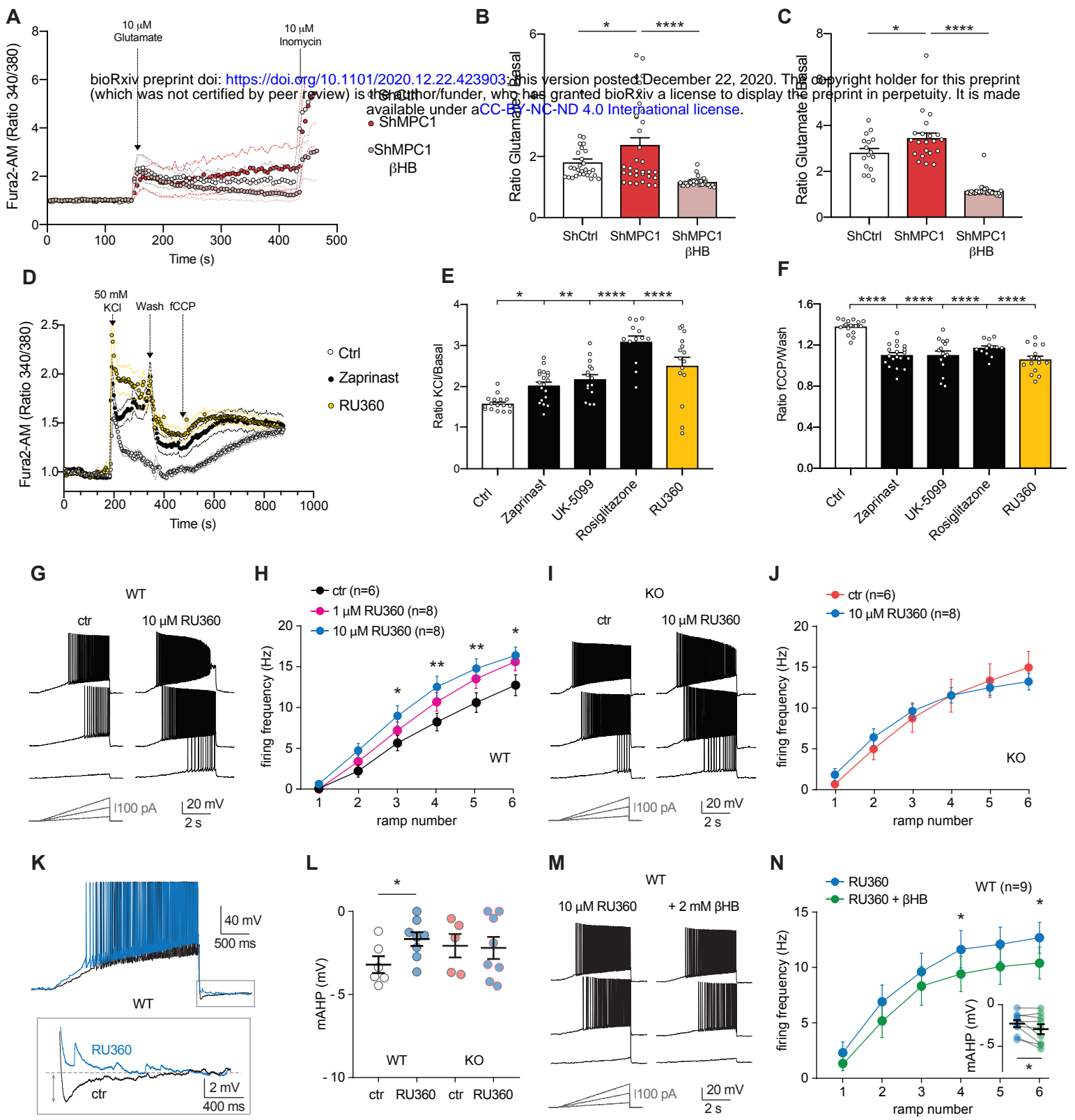


Figure 6